N-WASP coordinates the delivery and F-actin–mediated capture of MT1-MMP at invasive pseudopods

Xinzi Yu,[1] Tobias Zech,[1] Laura McDonald,[1] Esther Garcia Gonzalez,[2] Ang Li,[1] Iain Macpherson,[1] Juliane P. Schwarz,[1] Heather Spence,[1] Kinga Futó,[4] Paul Timpson,[1] Colin Nixon,[1] Yafeng Ma,[1] Ines M. Anton,[2] Balázs Visegrády,[4] Robert H. Insall,[1,3] Karin Oien,[3] Karen Blyth,[1] Jim C. Norman,[1,3] and Laura M. Machesky[1,3]

[1]The Beatson Institute for Cancer Research, Bearsden, Glasgow G61 1BD, Scotland, UK
[2]Centro Nacional de Biotecnologia (CNB-CSIC) Darwin 3, Campus Universidad Autónoma de Madrid Cantoblanco, 28049 Madrid, Spain
[3]College of Medical Veterinary and Life Sciences, University of Glasgow, Glasgow G12 8QQ, Scotland, UK
[4]Department of Biophysics, Medical School, University of Pécs, Pécs H-7624, Hungary

Metastasizing tumor cells use matrix metalloproteases, such as the transmembrane collagenase MT1-MMP, together with actin-based protrusions, to break through extracellular matrix barriers and migrate in dense matrix. Here we show that the actin nucleation–promoting protein N-WASP (Neural Wiskott-Aldrich syndrome protein) is up-regulated in breast cancer, and has a pivotal role in mediating the assembly of elongated pseudopodia that are instrumental in matrix degradation. Although a role for N-WASP in invadopodia was known, we now show how N-WASP regulates invasive protrusion in 3D matrices. In actively invading cells, N-WASP promoted trafficking of MT1-MMP into invasive pseudopodia, primarily from late endosomes, from which it was delivered to the plasma membrane. Upon MT1-MMP's arrival at the plasma membrane in pseudopodia, N-WASP stabilized MT1-MMP via direct tethering of its cytoplasmic tail to F-actin. Thus, N-WASP is crucial for extension of invasive pseudopods into which MT1-MMP traffics and for providing the correct cytoskeletal framework to couple matrix remodeling with protrusive invasion.

Introduction

Actin-driven cell shape alteration and migration as well as enzymatic modification of surrounding ECM are vital for tumor cells to invade and metastasize. Neural Wiskott-Aldrich syndrome protein (N-WASP) is a widely expressed member of the WASP/Scar family, which are major Arp2/3 complex-based actin nucleation–promoting proteins. N-WASP acts as a scaffold to coordinate signals from small GTPases, receptor tyrosine kinases, phospholipids, and SH3-domain–containing proteins to drive actin nucleation. Despite reports that N-WASP can promote filopod assembly (Miki et al., 1998), loss of N-WASP does not affect Cdc42-induced filopod formation in cultured primary fibroblasts, but modestly reduces clathrin-mediated endocytosis (Lommel et al., 2001). N-WASP is implicated in fission of endocytic vesicles and propelling vesicle departure from the plasma membrane (Taunton et al., 2000; Benesch et al., 2002; Merrifield et al., 2002), as well as the actin-driven dorsal ruffling that accompanies macropinocytosis (Legg et al., 2007). N-WASP is also implicated in lamellipodia generation in primary cultured Schwann cells (Jin et al., 2011). Thus, N-WASP–mediated actin nucleation contributes to plasma membrane protrusions and optimal function of both clathrin-dependent and clathrin-independent endocytosis (Yarar et al., 2007).

An emerging body of evidence suggests that N-WASP is linked with cancer progression and invasion. For example, N-WASP is up-regulated in metastatic liver lesions compared with primary colorectal tumors (Yanagawa et al., 2001). Interestingly, N-WASP (but not other WASP/Scar family members)

X. Yu and T. Zech contributed equally to this paper.

Correspondence to Laura M. Machesky: l.machesky@beatson.gla.ac.uk

Abbreviations used in this paper: BM, basement membrane; CIA, circular invasion assay; DCIS, ductal carcinoma in situ; FLIM, fluorescence-lifetime imaging microscopy; IAEDANS, 5-({2-[(iodoacetyl)amino]ethyl}amino)naphthalene-1-sulfonic acid; LE, late endosome; MMP, matrix metalloproteinase; NT, nontargeting; N-WASP, Neural Wiskott-Aldrich syndrome protein; PA, photoactivatable; PMT, photomultiplier tube; TMA, tissue microarray; WT, wild type.

The Rockefeller University Press $30.00
J. Cell Biol. Vol. 199 No. 3 527–544
www.jcb.org/cgi/doi/10.1083/jcb.201203025

is concentrated within invadopodia and is required for their formation (Lorenz et al., 2004; Yamaguchi et al., 2005; Oser et al., 2009). Additionally, N-WASP is important for the polarized formation of punctate structures, termed invadopodia precursors, in the leading edges of chemotaxing cells on 2D rigid glass substrates (Desmarais et al., 2009). The efficient function of invadopodia requires coordination of multiple machineries, including N-WASP–Arp2/3–mediated actin polymerization, cross-linking (fascin), maturation (cortactin), and accumulation of proteases such as matrix metalloproteinases (MMPs; Yamaguchi et al., 2005; Artym et al., 2006; Clark et al., 2007). However, the function of N-WASP in cancer cell migration and invasion has not yet been investigated in 3D ECM, nor has the effect of N-WASP depletion on trafficking of matrix degrading enzymes been investigated.

MMPs are multifunctional zinc-dependent endopeptidases involved in both signaling and matrix remodeling. Of this family, the membrane-anchored MT1-MMP is implicated both in the breaching of basement membranes (BMs) and in cell invasion through interstitial type-I collagen tissues (Sabeh et al., 2004; Hotary et al., 2006). MT1-MMP expression is correlated with the malignancy of multiple tumor types including lung, gastric, colon, breast, cervical carcinomas, gliomas, and melanomas (Seiki et al., 2003). Sabeh et al. (2004) have demonstrated that MT1-MMP serves as the dominant protease of both tumor cells and fibroblasts to degrade type-I collagen. Cells lacking MT1-MMP display no defects in 2D proliferation or migration across collagen-coated surfaces, but their capacity to invade is severely impaired (Sabeh et al., 2004). Cell surface MT1-MMP activity can be modulated by various routes, such as endocytosis (Jiang et al., 2001), recycling, autocatalytic processing, and posttranslational regulation (Ludwig et al., 2008; Poincloux et al., 2009). MT1-MMP accumulates at invadopodia and is important for focal degradation of ECM at these sites (Nakahara et al., 1997; Linder, 2007; Caldieri et al., 2009). Delivery and docking of MT1-MMP–containing vesicles at invadopodia requires membrane fusion machinery such as the vSNARE, VAMP7, and exocyst complex members as well as Rab8 (Bravo-Cordero et al., 2007; Steffen et al., 2008; Poincloux et al., 2009). Rab8 promotes polarized transport of newly synthesized membrane proteins in fibroblasts, and thus may control trafficking of newly synthesized MT1-MMP from the Golgi complex to the plasma membrane (Peränen et al., 1996). Here, we demonstrate that N-WASP–mediated actin polymerization drives invasive pseudopods, into which MT1-MMP is delivered, and we provide a novel F-actin–mediated mechanism for directed receptor targeting and stabilization of the invasive degrading machinery of cancer cells.

Results

N-WASP expression is increased in invasive breast cancer

To investigate the role of N-WASP in breast cancer invasion, we first assessed N-WASP expression in human breast cancer tissues. Normal breast, ductal carcinoma in situ (DCIS), and invasive ductal carcinoma were analyzed using immunohistochemistry to stain for N-WASP. N-WASP appeared weak, but showed specific cytoplasmic staining of epithelial cells in normal tissue and DCIS lesions. Knockdown cells prepared for histological analysis showed negative to weak staining in comparison with nontargeting (NT) control MDA-MB-231 (unpublished data). In contrast, N-WASP expression was up-regulated in invasive breast cancer samples (Fig. 1 A). To quantify N-WASP expression in human breast cancers, a tissue microarray (TMA; Biomax Z7020004) of 75 cores including normal/hyperplasia and tumor samples was stained and scored for N-WASP using the weighted histo-score method (see Materials and methods; Kirkegaard et al., 2006). N-WASP expression in invasive breast cancer was significantly higher than in normal or DCIS tissues ($P < 0.05$; Fig. 1 B). Furthermore, in normal mouse mammary glands, N-WASP consistently showed weak to moderate expression throughout various stages of mammary ductal homeostasis (Fig. 1 C), whereas mammary tumors from the MMTV-PyMT ($n = 9$) and MMTV-erbB2 (activated HER2, $n = 5$) mouse models (Muller et al., 1988; Fluck and Schaffhausen, 2009) consistently showed a dramatic increase in N-WASP expression (Fig. 1 D).

N-WASP drives cell elongation and the extension of long pseudopodia in 3D matrices

Most studies of N-WASP depletion have not revealed a role for N-WASP in peripheral lamellipodia extension or motility in 2D on rigid substrates (Snapper et al., 2001; Bryce et al., 2005; Kowalski et al., 2005; Misra et al., 2007; Sarmiento et al., 2008; Desmarais et al., 2009), although N-WASP has been implicated in filopodia (Hüfner et al., 2002; Bu et al., 2009) and lamellipodia formation in Schwann cells (Jin et al., 2011) and circular dorsal ruffles (Legg et al., 2007). We found that MDA-MB-231 invasive breast cancer cells depleted of N-WASP with two individual oligos by ∼90% using siRNA (Fig. S1 A) showed normal shape and motility parameters on a rigid 2D surface (Fig. S1, C and D). Protein levels of Scar/WAVE1, Scar/WAVE2, and WASH do not detectably change upon N-WASP depletion (Fig. S1 B). This suggests that in MDA-MB-231 cells, like most other cells studied to date, N-WASP does not have a detectable nonredundant role in motility on a 2D surface.

However, in 3D microenvironments, depletion of N-WASP dramatically affected the ability of MDA-MB-231 cells to invade in a 3D invasion assay where the cells crawled first through a filter (0 µM in Fig. 2 A) and then into a thick plug of Matrigel toward a gradient of serum with 25 nM of EGF (Hennigan et al., 1994). There was no difference between the N-WASP–depleted and NT cells in the number of cells that were able to migrate through the filter, which indicates that noninvasive migration was not impaired by N-WASP depletion. However, N-WASP–depleted cells showed greatly impaired invasive activity in Matrigel plugs, with invading cells reduced to around 10% (siN-WASP #1) and 30% (siN-WASP #2) compared with control (Fig. 2 A). To understand why cells depleted of N-WASP failed to invade, we first examined their morphology. In the inverted invasion assay, normal MDA-MB-231 cells elongated and formed elaborate long trains of cells connecting each other end-to-end and projecting into the Matrigel (Fig. 2 B and Video 1). N-WASP knockdown cells, in contrast, crossed over to the other side of the filter and then piled up as rounded cell aggregates that did not elongate or invade (Fig. 2 B and Video 2).

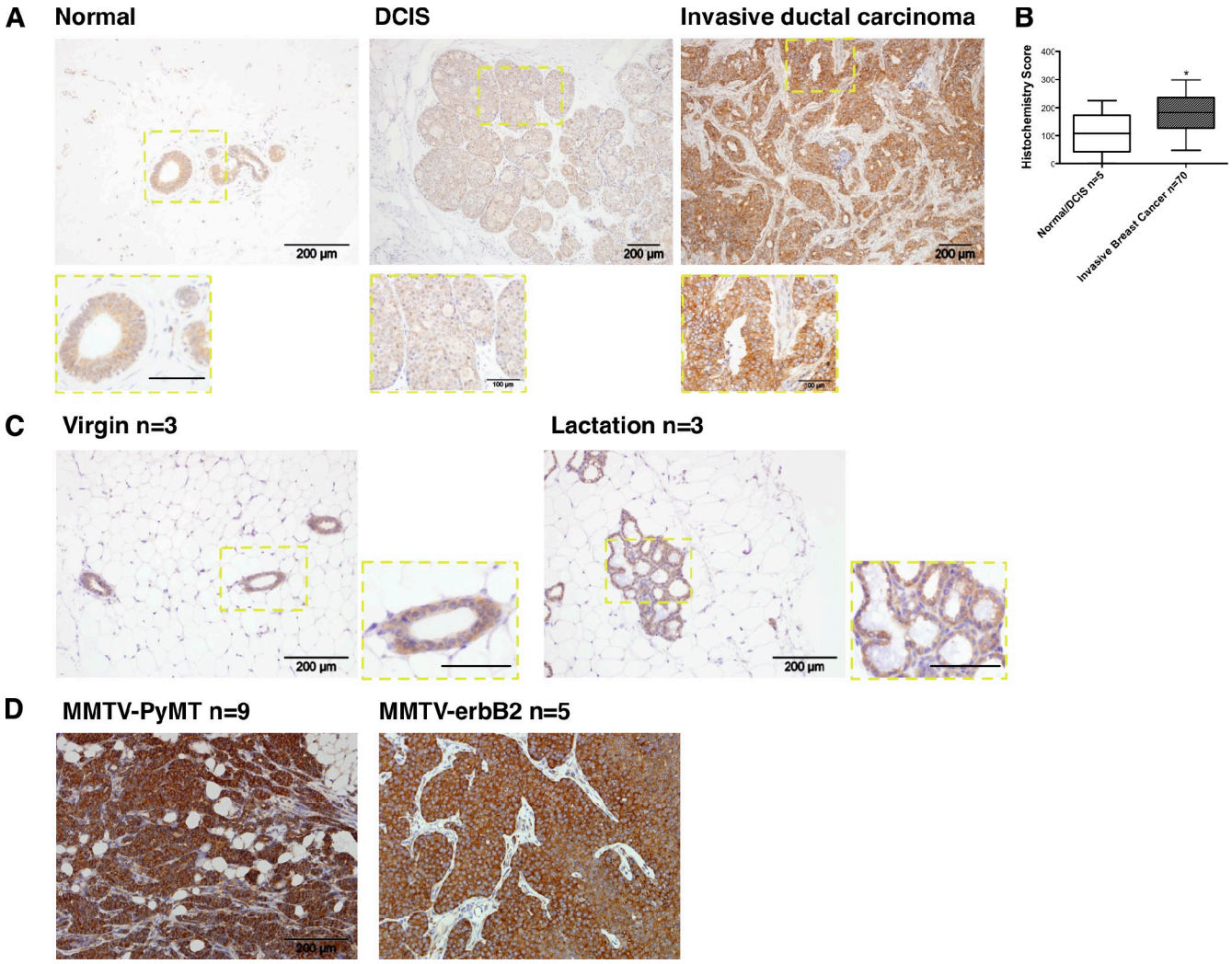

Figure 1. **N-WASP expression increases in both human and mouse invasive breast cancers.** (A) Immunohistochemical staining of N-WASP in human breast cancer tissues. Left and middle panels show expression of N-WASP in human normal tissue and DCIS. The right panel shows the expression level of N-WASP in human invasive ductal carcinoma. The insets show enlarged images of N-WASP staining in different tissues. (B) Bar graphs indicate histochemistry scores of normal/DCIS and invasive breast cancer cores from a 75-core human breast cancer TMA. All error bars indicate means ± SD; *, $P < 0.05$ by *t* test. (C) Immunohistochemical staining of N-WASP in mouse virgin and lactating mammary glands. Samples from three mice were stained and imaged. The insets show enlarged images of N-WASP staining in mouse virgin and lactating mammary glands. (D) Immunohistochemical staining of N-WASP in primary tumors from MMTV-PyMT ($n = 9$) and MMTV-erbB2 ($n = 5$) mouse models. Bars: (main panels) 200 μm; (insets) 100 μm.

N-WASP–depleted cells were also impaired in invasion in a modified version of the circular invasion assay (CIA; Kam et al., 2008), which enabled resolution of subcellular structures by both live cell time-lapse and fixed cell immunofluorescence (Fig. 3 A; Yu and Machesky, 2012). This assay is based on a wound-healing assay that is overlaid with Matrigel, and the cells invade into an empty space, rather than toward a specific attractant. Movement in the CIA was dependent on ECM remodeling, as knockdown of MT1-MMP, or inhibition with a broad MMP inhibitor, GM6001, reduced migration speed by 30–50% (Yu and Machesky, 2012). Similar to cells depleted for MT1-MMP, N-WASP–depleted cells (using two separate oligos siN-WASP #1 and siN-WASP #2) did not migrate far from the start point of the CIA (marked by black lines) and showed a 40% reduction of cell speed and persistence as analyzed with the ImageJ Chemotaxis Plugin (Fig. 3 A and Video 3).

In CIA, instead of extending elongated cylinder-like pseudopods, N-WASP–depleted cells displayed a threefold reduction in cell length/width ratio and small spiky protrusions (Fig. 3 B). However, dilution of the Matrigel with PBS (2.5 mg/ml Matrigel or 1.25 mg/ml Matrigel rather than the usual 5 mg/ml Matrigel) restored both migration velocity and directionality (Fig. 3 B and Video 4), which indicates that the Matrigel is providing a physical barrier to movement. In addition, the morphology of the knockdown cells in diluted Matrigel resembled the controls (longer pseudopodia and elongated shape; Fig. 3 B). Thus, we conclude that depletion of N-WASP in a 3D environment suppresses long pseudopod formation and invasion.

N-WASP is important for path generation during invasion in 3D matrix

During invasion, some cells become path-generating "leaders," which degrade matrices to lay down microtunnels for following

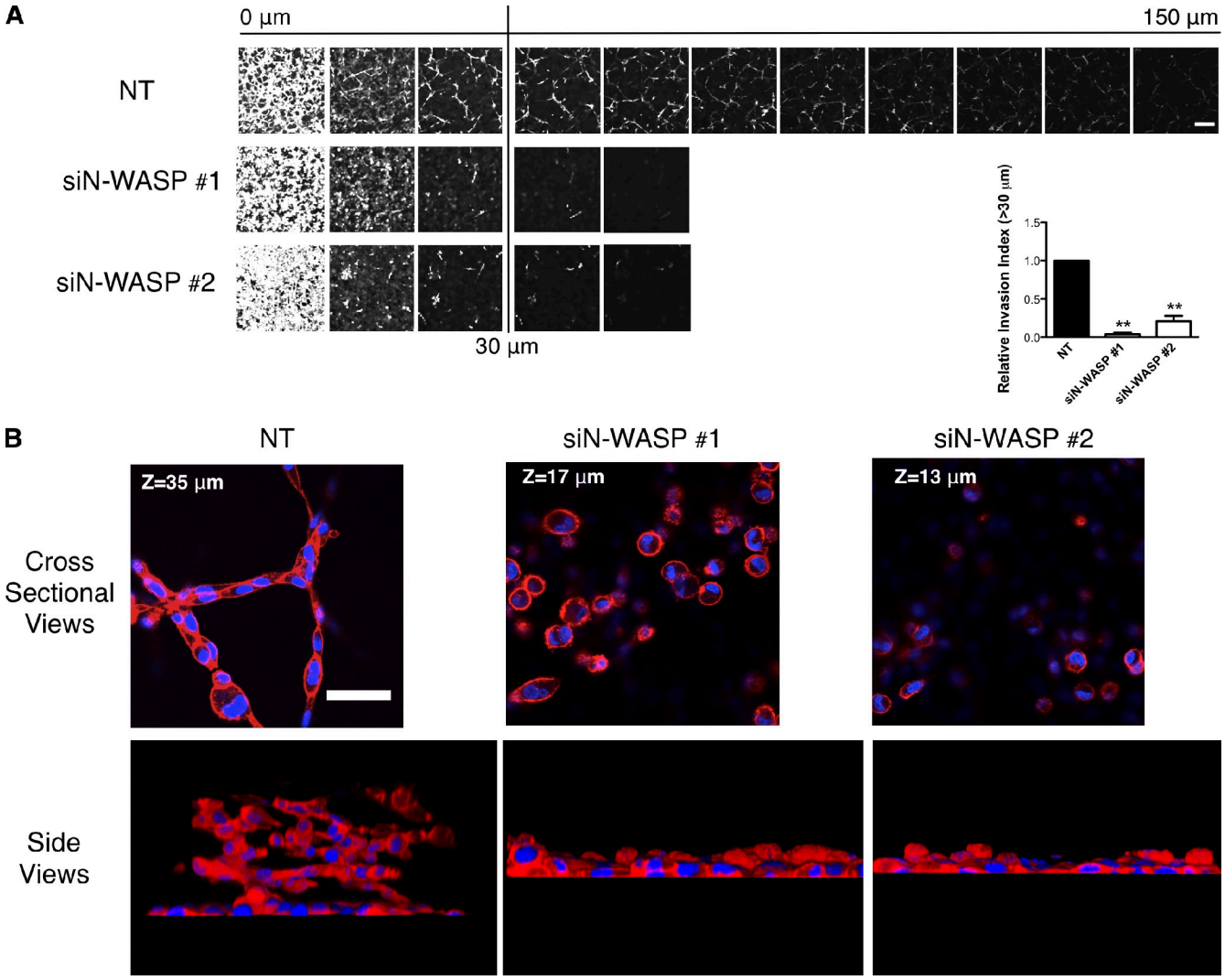

Figure 2. **N-WASP mediates leading cell collective invasion into 3D matrices.** (A) Cells that migrated into Matrigel plugs in an inverted invasion assay were stained with CalceinAM and visualized by confocal microscopy. Serial optical sections were captured at 15-µm intervals and presented as a sequence in which the individual optical sections are placed alongside one another, with increasing depth from left to right as indicated. The assays were quantified by measuring the fluorescence intensity of cells penetrating 30 µm and greater. 0 µm indicates cells that crawled through the filter but did not enter the gel. The invasion capacity was expressed as a percentage of the total fluorescence intensity of all cells within the plug, as shown in the bar graph. At least three independent experiments were performed. All error bars indicate means ± SD; **, $P < 0.01$ by a *t* test. Bar, 100 µm. (B) Matrigel plugs containing cells from inverted invasion assays were fixed and stained with phalloidin (actin, red) and DAPI (DNA, blue). Strands of invading cells are shown in cross section and side views. Bar, 50 µm.

cells (Fisher et al., 2009; Scott et al., 2010). If the function of N-WASP was to be limiting for matrix remodeling, but not for movement or chemotaxis in 3D matrix, nor for joining together with other cells in an invasion stream, we would expect that addition of normal cells together with N-WASP–depleted cells might rescue the invasion defect caused by N-WASP depletion. Indeed, in both the CIA (Fig. 4 A) and the inverted invasion assay (Fig. 4 C), addition of normal (GFP-expressing, NT siRNA–transfected) green cells to red N-WASP knockdown (RFP-expressing, siN-WASP–transfected) cells significantly rescued the invasion defect of the N-WASP knockdown cells (Fig. 4, A and C). In a mixed population of GFP- and RFP-expressing NT cells, the green and red cells showed a roughly 50:50 ratio as leading or following cells, as the white arrowheads indicate in Fig. 4 (A, left, and B). However, in ∼90% of invasion strands, GFP-expressing NT cells are the path-generating "leader" cells when mixed with RFP-siN-WASP cells (Fig. 4 A, right, white arrowheads; and Fig. 4 B). N-WASP–depleted (red) cells rarely assumed the position as a leader in the invasion front, and they were less elongated than the NT cells (Fig. 4, A and C). Consistently, in the inverted invasion assay, RFP-expressing siN-WASP cells displayed impaired invasion, but invaded nearly normally when mixed with GFP-NT cells (Fig. 4 C). Therefore, we conclude that N-WASP–depleted cells are unlikely to have a defect in movement in 3D matrix, but they are impaired in the formation of elongated pseudopodia and path generation.

N-WASP knockdown cells are defective in matrix degradation by MT1-MMP

To directly address the possibility that N-WASP–depleted cells were defective in matrix remodeling, we explored their ability to remodel uncrosslinked collagen (Sabeh et al., 2004; Wolf

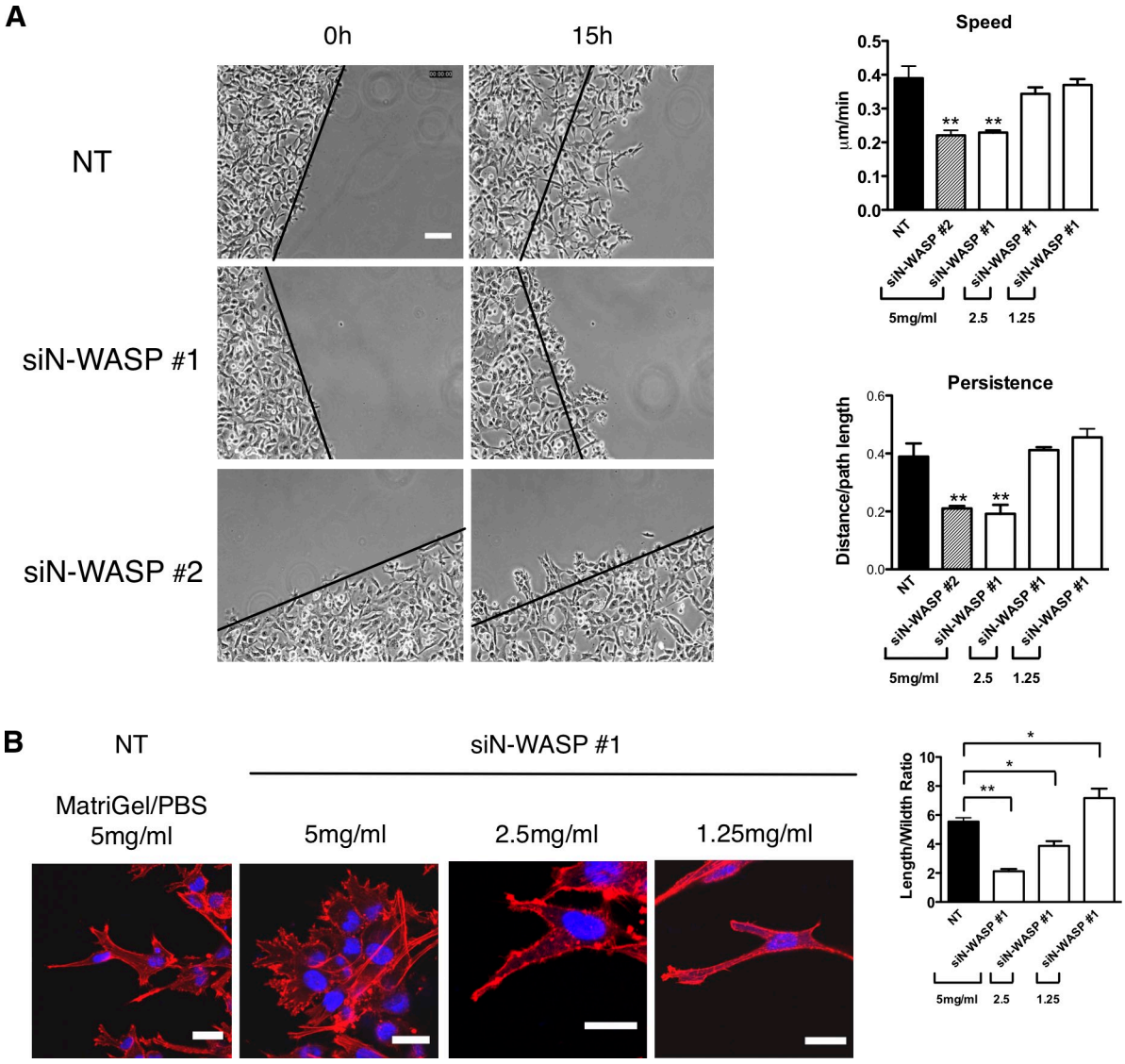

Figure 3. **N-WASP is required for extension of elongated matrix degrading pseudopods and propulsion through dense matrix.** (A) MDA-MB-231 cells treated with siRNA NT and N-WASP invading under Matrigel (photos show 5 mg/ml Matrigel, bar graphs show concentrations as indicated) in a CIA. Black lines indicate the start of the cell front at t = 0 h. Cell migration speed and persistence in CIA are shown in the bar graph. Persistence is obtained by using the Euclidean distance divided by the total distance between the start and end points of cell movement. At least three independent experiments were performed and quantified. Error bars indicate means ± SD; **, P < 0.01 by *t* test. Bar, 100 μm. (B) Cells invading in CIA were fixed and stained with phalloidin (actin, red) and DAPI (DNA, blue) for confocal imaging. The length of actin pseudopods and the ratio of cell length/width in CIA are shown in the bar graph. Error bars indicate means ± SD; **, P < 0.01; *, P < 0.05 by *t* test. At least 30 cells were analyzed in three independent experiments. Bars, 20 μm.

et al., 2007) and native cross-linked BMs (Hotary et al., 2006). When NT control cells were plated onto thin uncrosslinked collagen matrix, they rapidly degraded large areas of matrix underneath the cell (Fig. 5 A; Sabeh et al., 2004). However, knockdown of MT1-MMP or N-WASP nearly completely prevented this remodeling (Fig. 5 A; Sabeh et al., 2004). In a more quantifiable assay, where the cells were embedded in a collagen matrix containing DQ collagen (Wolf et al., 2007), the amount of degradation of DQ collagen was reduced by 40–50% upon inhibition or knockdown of MT1-MMP or N-WASP (Fig. 5 B). We next analyzed the ability of cells to degrade native peritoneal BM as described previously (Hotary et al., 2006). This isolated BM appears as two layers of continuous and organized sheets of type IV collagen- and laminin-rich ECM flanked by a layer of stroma. MDA-MB-231 cells transfected with a NT siRNA were able to degrade BM collagen IV efficiently within the 3-d culture period. However, N-WASP–depleted cells left the BM collagen IV relatively unscathed (Fig. 5 C). Quantification of the remaining collagen IV staining intensity shows a 50% reduction of matrix remodeling by siN-WASP cells compared with control (Fig. 5 D). Likewise, siRNA depletion of MT1-MMP or addition of 5 μM GM6001 significantly blocked the ability of MDA-MB-231 cells to degrade and remodel the BM collagen IV as described previously (Fig. 5, C and D; Kowalski et al., 2005; Chun et al., 2006). Collectively, these data provide clear and direct evidence that N-WASP has a role in matrix degradation and contributes to the breakdown of physiological BMs such as would be encountered in a tumor environment.

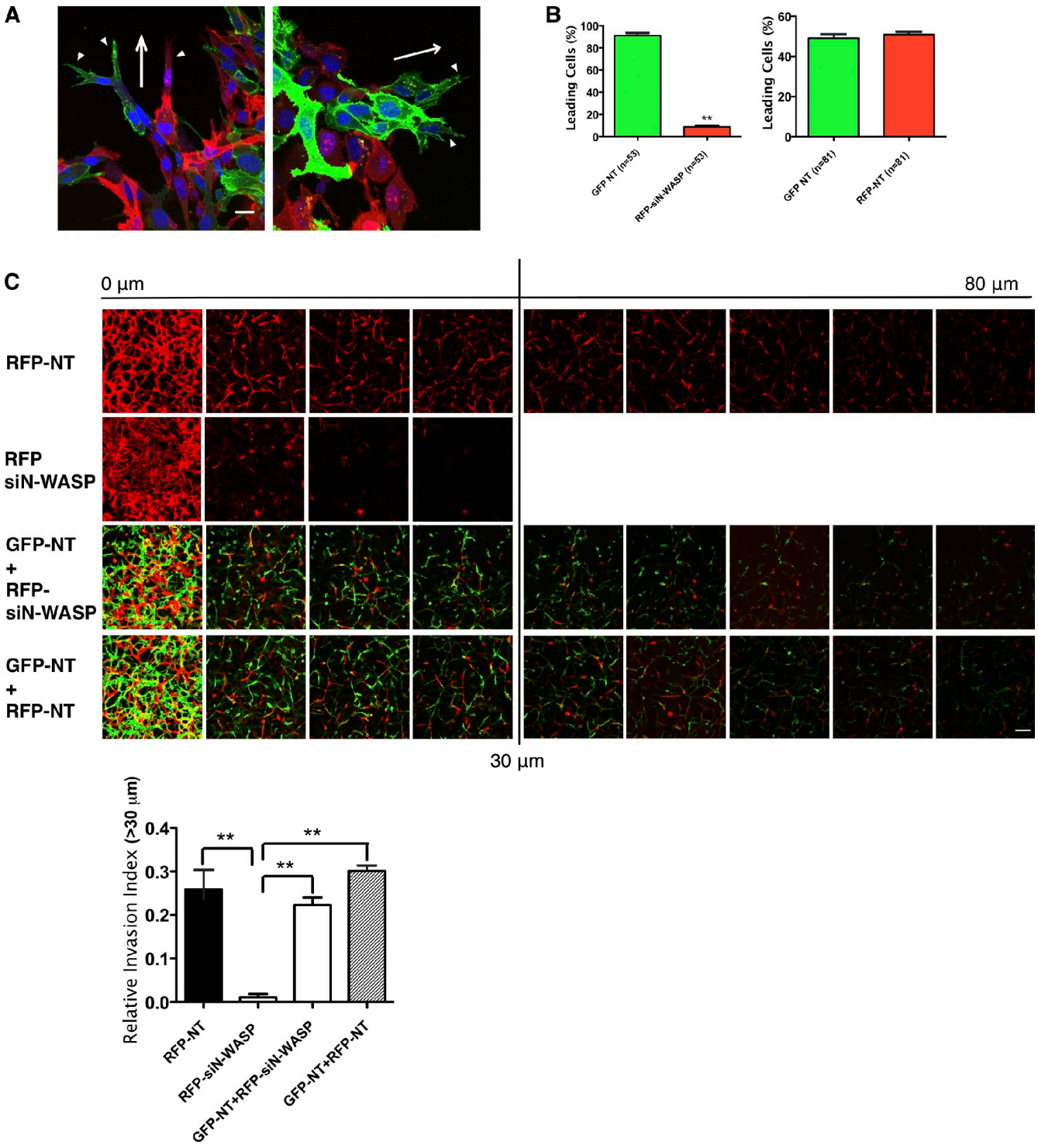

Figure 4. **N-WASP is required for path generation during invasion.** (A) Equal numbers of RFP-expressing cells transfected with either NT or N-WASP siRNA (red) were mixed with GFP-labeled cells treated with NT siRNA (green) in CIA. Cells were fixed and stained for DNA (blue) to show path-generating and following cells in the invading strands. Arrowheads indicate leading cells of invasive cell strands. Arrows indicate the direction to the wound edge. At least three independent experiments were performed and quantified. Bar, 10 µm. (B) Bar graphs indicate the percentage of leading and total cells of GFP- and RFP-positive cells. Error bars indicate means ± SD; **, $P < 0.01$ by *t* test. (C) A similar setup was used as in A, except that NT or N-WASP siRNA RFP-expressing cells alone were seeded for inverted invasion assay. Serial optical sections were captured at 10-µm intervals and presented as a sequence in which the individual optical sections are placed alongside one another with increasing depth from left to right as indicated. Images at 0 µm indicate cells that came though the filter but did not enter the gel. Invasion capacity was expressed as a percentage of the total fluorescence intensity of all cells invading beyond 30 µm within the plug as shown in the bar graph. At least three independent experiments were performed and quantified. Bar, 100 µm.

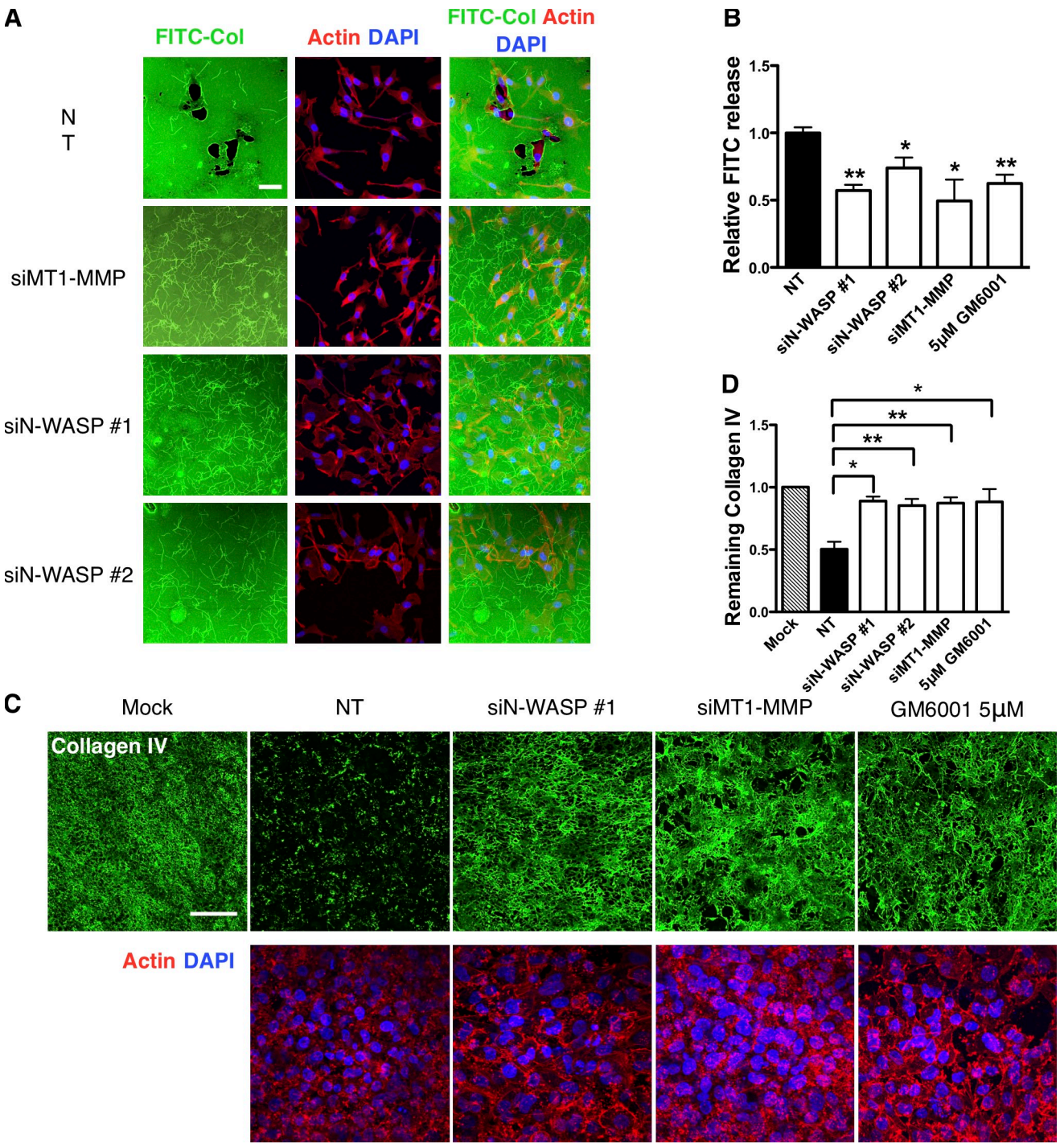

Figure 5. **N-WASP is crucial for pericellular collagenolysis in vitro and on native BMs.** (A) Immunofluorescence images of cells on FITC-conjugated type-I collagen film (green). Cells were labeled for filamentous actin (red, phalloidin) and DNA (blue, DAPI). Bar, 50 µm. (B) Quantification of FITC fluorescence release after incubating cells with DQ collagen matrix from three independent experiments. (C) MDA-MB-231 cells were cultured atop of mouse peritoneal BM for 3 d and then fixed and stained for collagen IV (green), actin (phalloidin, red), and DNA (DAPI, blue). The cells remodel and degrade BM, and the remaining collagen IV is shown by antibody staining (green). Bar, 100 µm. (D) The total fluorescence intensity of remaining collagen IV is represented in the bar graph. At least three independent experiments were performed and quantified. Error bars indicate means ± SD; **, $P < 0.01$; *, $P < 0.05$ by *t* test.

N-WASP drives invasive pseudopods into which MT1-MMP traffics from Rab7-positive late endosomes (LEs)

Because loss of N-WASP inhibited MT1-MMP dependent matrix degradation, we hypothesized that actin-rich regions of invasive pseudopods might be sites of MT1-MMP trafficking (Frittoli et al., 2011). To first address whether N-WASP played a direct role in MT1-MMP protein levels, internalization, or recycling, we measured total and surface levels of MT1-MMP, rates of internalization, and recycling, and found no effect of N-WASP depletion (Fig. S2, A–C). We next hypothesized that N-WASP likely has a more indirect role in trafficking and may

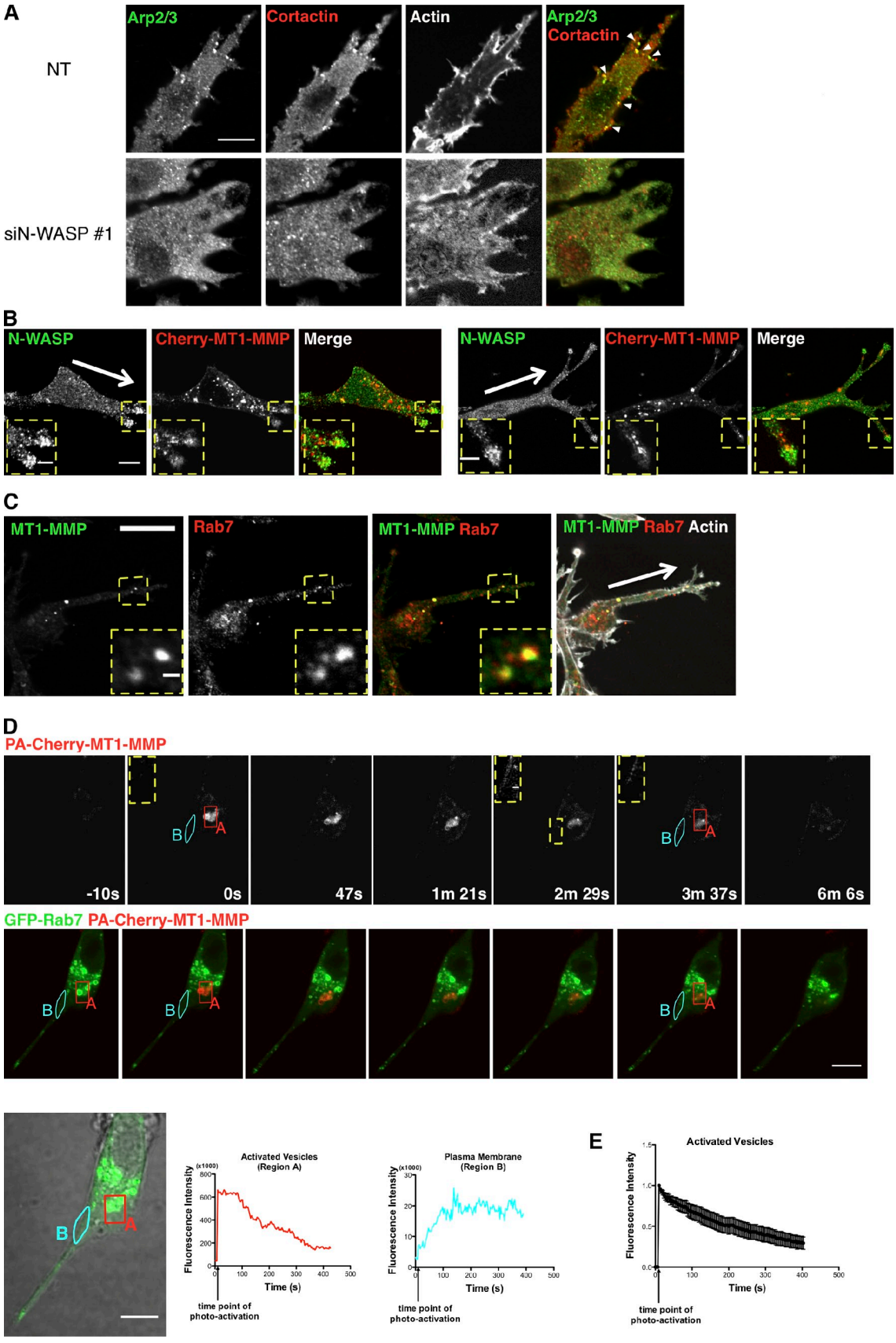

Figure 6. **MT1-MMP traffics from a late endosomal compartment to the plasma membrane and associates with N-WASP.** (A) NT and N-WASP knockdown cells invading in CIA were fixed and stained with anti-Arp2/3 and cortactin to reveal actin-rich puncta (arrowheads) in NT cells (top). (B) Immunofluorescence images of invading cells expressing mCherry-MT1-MMP (red) and staining for endogenous N-WASP (green) in CIA, with arrows pointing toward the wound edge. Bar, 10 µm. Enlarged images show details (boxed regions) of the invasive pseudopods containing MT1-MMP vesicles and N-WASP puncta.

promote MT1-MMP to preferentially traffic into invasive pseudopodia, and to be stabilized at sites of invasive matrix remodeling. The leading pseudopods of invading NT cells displayed numerous N-WASP–dependent puncta rich in cortactin, actin, N-WASP, and Arp2/3 complex, and also showed degradation of nearby surrounding matrix (Fig. 6 A; Yu and Machesky, 2012). Notably, these puncta, which contacted the Matrigel, also contained vinculin (82%, n = 17 cells) and focal adhesion kinase (74%, n = 12 cells; Fig. S3). But as previously reported (Yu and Machesky, 2012), cells also displayed some puncta at the glass bottom surface that lacked N-WASP but were rich in vinculin and FAK, which we assume were focal adhesion structures (Fig. S3). MT1-MMP also partially colocalized with N-WASP in the matrix contacting cytoskeletal puncta (Yu and Machesky, 2012), and we frequently observed vesicles containing MT1-MMP directly trafficking into invasive pseudopods in CIA. These vesicles often localized adjacent to the puncta rich in N-WASP or overlapped with the N-WASP–rich invadopodia-like structures (Fig. 6 B). Thus, we conclude that the majority of N-WASP– and Arp2/3 complex–rich puncta that we observed in invasive pseudopodia in the CIA also contained FAK and vinculin, and were most likely hybrid invadopodia/focal adhesion structures formed by a coalescence of these structures, which are more distinct in 2D (Wang and McNiven, 2012).

Additionally, a significant portion of MT1-MMP could be found in intracellular vesicles. Co-labeling with endocytic markers revealed that the majority of this vesicular MT1-MMP was in a Rab7- and CD151-positive LE compartment, which is in agreement with previous studies showing localization of MT1-MMP to a VAMP7-positive compartment (Fig. 6 C and Fig. S4 A; Steffen et al., 2008). We also saw partial colocalization with Rab8, in agreement with previous studies (unpublished data; Bravo-Cordero et al., 2007). Using live-cell video microscopy, we found that MT1-MMP cotrafficked bi-directionally in invasive pseudopods together with Rab7 and CD151, but not the early endosome marker Rab4 (Fig. S4 A and Video 5). The trafficking into invasive pseudopods was affected by loss of N-WASP, as >70% of NT cells contained five or more MT1-MMP vesicles within the pseudopods (n = 23; Fig. S4 B), whereas N-WASP–depleted cells (>90%) had fewer MT1-MMP vesicles within these structures (n = 41; Fig. S4 B). Because only a few studies have shown trafficking back to the plasma membrane from the LE compartment (Zech et al., 2011; Dozynkiewicz et al., 2012), we tested whether the LE vesicles that were rich in MT1-MMP were capable of delivering MT1-MMP to the plasma membrane, or were rather only involved in its degradation. We constructed a photoactivatable mCherry-tagged MT1-MMP (PA-mCherry-MT1-MMP) to follow MT1-MMP dynamics in live cells during the invasion process. We used GFP-Rab7 as a marker for the LE compartment, and when we photoactivated Rab7-positive vesicles, we initially observed a flash of PA-mCherry-MT1-MMP on this compartment, which subsequently redistributed to the nearby plasma membrane (Fig. 6 D and Video 6). We measured the time course over which photoactivated PA-mCherry-MT1-MMP fluorescence was lost from Rab7 vesicles, and found that this corresponded to the subsequent increase of fluorescence on the nearby plasma membrane (Fig. 6 D, graphs). The fluorescence intensity of the activated vesicles was recorded in multiple cells (n = 10) and plotted in Fig. 6 E, where we can see clearly that the PA-mCherry-MT1-MMP exits quickly from the Rab7 compartments upon activation. Thus, a proportion of the MT1-MMP in the Rab7-positive LE vesicles that we observe in invading cells is in transit to the plasma membrane from this compartment. We were not able to measure traffic specifically into the tips of invasive pseudopodia (rather than generally to the nearby plasma membrane) because the signal from PA-mCherry-MT1-MMP was not bright enough.

A link formed between MT1-MMP and actin contributes to delivery and stabilization of MT1-MMP at the plasma membrane of invasive pseudopods

To determine whether N-WASP contributed to entrapment of MT1-MMP at pseudopod tips, we investigated the dynamic behavior of MT1-MMP within invasive structures. We hypothesized that the cytoplasmic tail of MT1-MMP might connect to the actin cytoskeleton and thus be tethered in actin networks generated by N-WASP in invasive pseudopodia. We performed photobleaching experiments to test whether MT1-MMP at the plasma membrane in invasive pseudopodia had reduced mobility compared with MT1-MMP in other regions of the cell surface (e.g., at the plasma membrane adjacent to the nucleus). Photobleaching of mCherry-MT1-MMP in invading pseudopod tips in matrix of control NT-transfected cells revealed a very low, 5%, mobile fraction, indicating that nearly 95% of the enzyme doesn't exchange with the neighboring plasma membrane and isn't replaced by vesicular trafficking within the time frame of our experiment (1 min; Fig. 7, A and B). Indeed, the photoactivation experiments in Fig. 6 indicate that the delivery of PA-mCherry-MT1-MMP to the plasma membrane occurs over a period of several minutes, not seconds. In contrast, 22 ± 4% of mCherry-MT1-MMP on the cell body

(C) Endogenous MT1-MMP vesicles colocalize with endogenous Rab7. Arrows point toward the wound edge. Bar, 20 µm. Inset images show the LE/LY vesicles containing both MT1-MMP and Rab7 (enlarged views of the boxed regions). (D) MDA-MB-231 cells expressing PA mCherry-MT1-MMP (red) and GFP-Rab7 (green) were plated in CIA and imaged by confocal microscopy. Photo-activation was achieved with a 405-nm laser aimed at a small area (region A) containing GFP-Rab7–positive vesicles (also MT1-MMP), marked by the red box. Images were then captured at 3.2 s per frame over a period of >6 min (Video 6). Single-section confocal images of activated mCherry-MT1-MMP and images of merged mCherry-MT1-MMP and GFP-Rab7 at certain time points were presented. The insets are enlarged images showing increased signals of photoactivated mCherry-MT1-MMP on the plasma membrane area near the activated vesicles. The enlarged area is indicated with the yellow dotted line at time point "2 m 29 s." The same areas are shown in time points "0 s" and "3 m 37 s." The integrated fluorescence intensity of activated region A (red) and a area of plasma membrane (region B) near the activated vesicles (light blue) was quantified for each frame of Video 6, and the values are plotted against elapsed time. (E) Quantification of fluorescence intensity of activated mCherry-MT1-MMP vesicles in multiple experiments indicated the exit rate of photoactivated mCherry-MT1-MMP from the Rab7-positive compartment (n = 10). Error bars indicate means ± SEM. Bars: (A) 20 µm; (B) 5 µm; (C) 1 µm; (D) 10 µm; (B–D, insets) 1 µm.

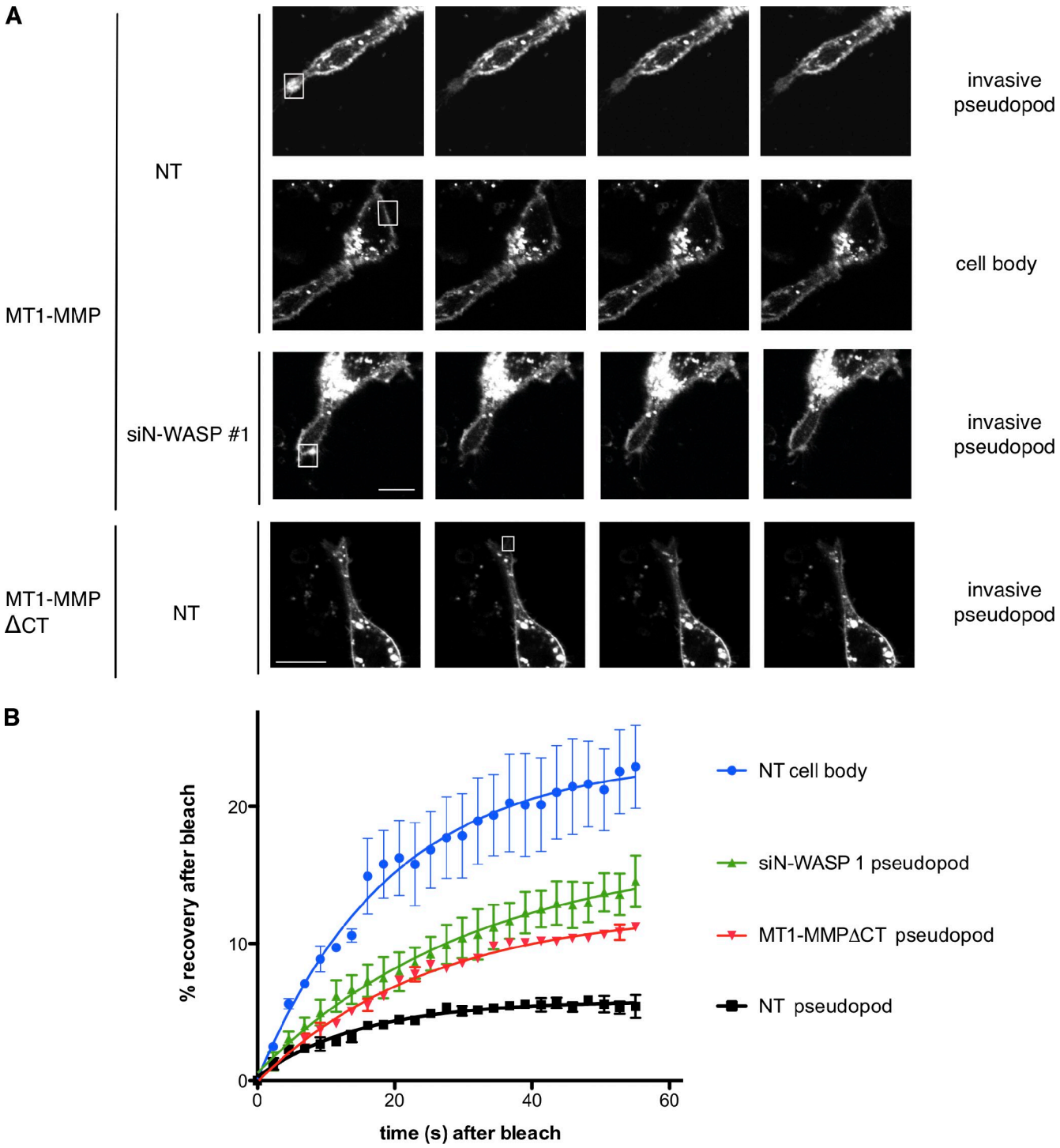

Figure 7. **MT1-MMP is tethered to invasive pseudopods in an N-WASP–dependent manner.** (A) MDA-MB-231 were transfected with mCherry-MT1-MMP or mCherry-MT1-MMPΔCT, as indicated, as well as GFP-actin, and subjected to CIA. Selected actin-rich areas in invasive pseudopods or areas of the cell body (boxes shown in A and quantified in B) of NT or N-WASP–depleted cells as indicated were photobleached using a 405-nm laser, and recovery of mCherry-MT1-MMP fluorescence was recorded for 58 s. (B) Quantification of fluorescence recovery was of at least 30 cells in three independent experiments. Error bars indicate means ± SEM. Bar, 10 µm.

plasma membrane is mobile and recovers quickly ($t_{1/2}$ = ~15 s) after bleaching (Fig. 7, A and B). Depletion of N-WASP, which causes loss of actin-rich hotspots and blunting of pseudopods, led to an increase of the mobile MT1-MMP fraction in pseudopods to 15 ± 3% compared with NT-transfected cells (Fig.7, A and B). Thus we conclude that N-WASP is important for stabilizing MT1-MMP in invasive pseudopods, possibly via assembly of dense actin meshworks in these structures. These invasive pseudopods not only need to generate mechanical force to push and pull against the matrix, but also direct and sustain MT1-MMP–based degradation. To demonstrate such an inside-out mechanism of MT1-MMP capture, we analyzed

the mobile fraction of MT1-MMP-ΔCT (MT1-MMP without its cytoplasmic domain), which is ineffective at rescuing (Uekita et al., 2001). We found that MT1-MMP-ΔCT has an increased mobile fraction of ∼12% compared with around 5% for full-length mCherry-MT1-MMP in invasive pseudopods of NT cells (Fig. 7, A and B). To further explore the role of actin networks in stabilization of MT1-MMP in invasive pseudopodia, we treated cells either with siRNA against Arp2 to block Arp2/3 complex–mediated actin assembly or with 2 µM Latrunculin A to partially depolymerize filamentous actin (Fig. S5, C and D). In both cases, mCherry-MT1-MMP became more mobile in the plasma membrane of remaining pseudopodia in Matrigel. The observation that GFP-actin exchanged much faster in LatA-treated cells (Fig. S5 E) verified that the LatA mobilized the actin network as expected. Thus, branched actin networks formed by Arp2/3 complex and filamentous actin stabilize MT1-MMP in pseudopods.

Because it has been recently highlighted that some receptors can be sorted on membranes putatively via links with actin filament networks (Puthenveedu et al., 2010), we hypothesized that MT1-MMP might directly interact with F-actin, and we tested whether binding to F-actin could determine MT1-MMP mobility on the plasma membrane. We first performed biochemical experiments to see if F-actin could deplete soluble peptides corresponding to the MT1-MMP tail from the supernatants in a centrifugation experiment. MT1-MMP wild-type (WT) cytoplasmic tail or peptides of cytoplasmic tail where the LLY motif, previously found to be important for MT1-MMP to confer invasiveness (Uekita et al., 2001), was exchanged to AAA (labeled as LLY/A in the figures) were incubated with F-actin purified from rabbit muscle. Actin filaments readily depleted MT1-MMP cytoplasmic tail peptides but not mutant LLY/A peptides from the supernatants (Fig. 8, A–D). We further explored the specificity of the interaction of the MT1-MMP tail peptide with actin filaments using a fluorescence anisotropy experiment (see Materials and methods), where fluorescently labeled short actin filaments were incubated with soluble peptides corresponding to either WT or mutant LLY/A MT1-MMP tail or a scrambled peptide of the MT1-MMP tail that preserves the overall positive charge of the WT peptide (Fig. 8 E). Fluorescence anisotropy also revealed specific binding to the WT with a K_d = 43 ± 6.5 µM, but not the mutant peptides, which suggests that the LLY motif was important for the interaction between MT1-MMP and actin filaments.

To further investigate whether the interaction between F-actin and MT1-MMP could also be observed in living cells, we transfected MDA-MB-231 cells with MT1-MMP-GFP and Lifeact-TagRFP to measure fluorescence-lifetime imaging microscopy (FLIM) in invasive pseudopods. Cells transfected only with the MT1-MMP-GFP donor showed an average fluorescence lifetime of 2.4 ns at the tips of invasive pseudopods. In contrast, cells containing both the MT1-MMP-GFP donor and Lifeact-TagRFP as an acceptor showed a significant shift of 150 ps in the fluorescence lifetime of MT1-MMP-GFP to 2.25 ns (Fig. 8 F), thus confirming that the cytoplasmic tail of MT1-MMP has the ability to interact with actin in invasive pseudopods. Mutation of the LLY motif to AAA also abolished the FLIM signal (Fig. 8 F) and increased the motility of the protease in invasive pseudopods in the FRAP experiment (Fig. S5, F and G), thus demonstrating that this interaction is dependent on this motif in cells (Fig. 8 F). We also further investigated the ability of MT1-MMP with the LLY/AAA mutation to drive invadopodia assembly (Fig. 8 G). Although WT MT1-MMP could rescue cells depleted of MT1-MMP by siRNA, the LLY/A mutant MT1-MMP was unable to rescue. Likewise, LLY/A mutant MT1-MMP was unable to rescue the reduction of invasion observed in the circular Matrigel invasion assay (Fig. S5, A and B; Yu and Machesky, 2012).

To investigate whether F-actin binding of MT1-MMP in invasive pseudopods is necessary and sufficient for a cell to increase invasion, we replaced the cytoplasmic tail of MT1-MMP with the actin-binding domain of ezrin (aa 552-585; MT1-MMP$^{EZ\text{-}ABD}$) and compared the invasion and invadopodia formation with cells transfected with either MT1-MMP or MT1-MMP ΔCT. The mCherry-MT1-MMP$^{EZ\text{-}ABD}$ construct shows similar distribution to WT MT1-MMP, with a slightly increased intracellular pool (Fig. 8 G). We also compared the mobility of WT mCherry-MT1-MMP and mCherry-MT1-MMP$^{EZ\text{-}ABD}$ in invasive pseudopods using FRAP and did not find any significant difference in the mobility of these proteins (Fig. S5 G). For invadopodia degradation assays, we first depleted endogenous MT1-MMP using siRNA against the 5′ untranslated region in MDA-MB-231 cells and then transfected WT and mutant MT1-MMP into them. Consistently, full-length MT1-MMP dramatically increased MDA-MB-231 cell degradation on a thin layer of gelatin (Fig. 8 G), which agrees with previous work (Nakahara et al., 1997). The actin-binding domain mutant of MT1-MMP (mCherry-MT1-MMP$^{EZ\text{-}ABD}$) was able to promote matrix degradation in a similar fashion (Fig. 8 G). In contrast, MT1-MMP-ΔCT– and MT1-MMP-LLY/A–expressing cells barely show any gelatin degradation (Fig. 8 G). Collectively, these observations indicate that the capacity of the cytoplasmic tail to recruit MT1-MMP to the subplasmalemmal actin cytoskeleton facilitates the concentration of MT1-MMP at actin-enriched sites to confer effective matrix degradation during invasion.

Discussion

N-WASP had been previously described as a component of invadopodia and their precursor structures, but the molecular mechanism of how N-WASP drives invasion hasn't been studied in 3D (Lorenz et al., 2004; Yamaguchi et al., 2005). N-WASP has recently been implicated in breast cancer metastasis in a mouse model (Gligorijevic et al., 2012). Here we provide a direct mechanism by which N-WASP drives invasive migration via the generation of elongated pseudopods that allow cells to remodel matrix and generate force to crawl through it. Although N-WASP and its hematopoietic homologue WASP have been implicated in chemotaxis on a 2D surface (Isaac et al., 2010), we did not find any evidence of significantly reduced noninvasive migration of N-WASP–depleted cells through filters in 3D (Fig. 2). Furthermore, when we diluted Matrigel in the CIA (Fig. 3), this restored the migration speed of

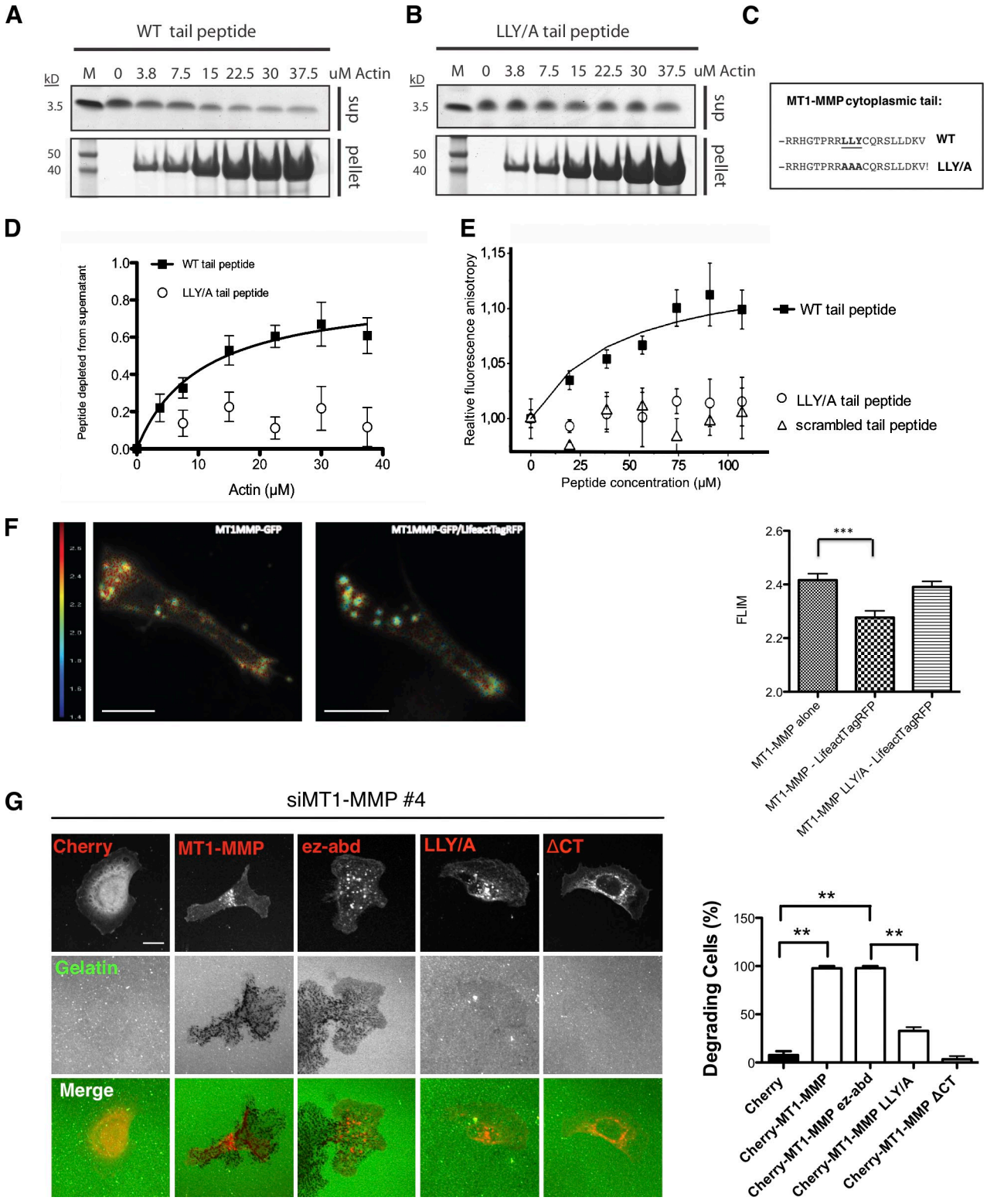

Figure 8. **MT1-MMP actin binding is both necessary and sufficient to induce matrix degradation.** (A–C) 25 µM final concentration of WT (A and C) cytoplasmic MT1-MMP tail peptide or LLY/AAA (B and C) cytoplasmic MT1-MMP tail peptide were tested for their ability to bind to increasing amounts of F-actin in an in vitro binding assay. Actin was allowed to polymerize for 1 h. After centrifugation, 10% of total F-actin pellets (p) and supernatants (s) were run on a 4–12% NuPAGE gel using MES running buffer. (D) Quantification of Coomassie gel densitometry of peptide bands. $n = 5$. (E) Relative steady-state fluorescence anisotropy was measured between IAEDANS-labeled filamentous actin (2 µM) and increasing concentration of MT1 peptide constructs: MT1_tail (closed squares), MT1tail_L1Y/A (open circles), and MT1tail_scrambled (open triangles). The binding curve was fitted with the equation given in the Materials and methods section ("Steady-state fluorescence anisotropy experiments"), and the K_d value was calculated (see Results). (F) MDA-MB-231 cells were transfected with MT1-MMP-GFP alone or together with Lifeact-TagRFP and invaded in Matrigel in CIA. Cells were imaged using a spinning disc FLIM system. Fluorescence lifetime was measured in the pseudopod area and quantified from 30 cells in $n = 3$. Bar, 10 µm. (G) Immunofluorescence images of mCherry, mCherry-MT1-MMP, mCherry-MT1-MMPΔCT, and mCherry-MT1-MMP$^{EZ\text{-}ABD}$ expressing MDA-MB-231 MT-MMP knockdown cells (red) on

N-WASP–depleted cells to normal, which indicates that migration through Matrigel was not likely hindered by a loss of the ability of N-WASP–depleted cells to generate a gradient of the growth factor components found in Matrigel. Finally, when we mixed N-WASP–depleted cells 50:50 with normal NT controls, this rescued invasion into thick gels, and N-WASP–depleted cells rarely participated as "leader cells" in the invasion chains (Fig. 4). Thus, we conclude that N-WASP contributes to the formation of elongated protrusions rich in actin cytoskeletal components (F-actin, cortactin, and Arp2/3 complex), and that these protrusions are required to overcome the physical barrier to cell translocation provided by ECM.

The main morphological defects of N-WASP–depleted cells migrating in 3D included blunted pseudopods, loss of actin-rich punctae, and reduced numbers of MT1-MMP vesicles in leading pseudopodia. MT1-MMP has previously been implicated as a Rab8 vesicle cargo (Bravo-Cordero et al., 2007). Although we saw overlap of MT1-MMP with the Rab8 compartment, the overwhelming majority of MT1-MMP vesicular structures that we saw were Rab7 positive. This agrees with a previous study also showing colocalization of MT1-MMP with a VAMP7-positive compartment (Steffen et al., 2008). Although it may seem surprising that MT1-MMP largely recycles from a Rab7-positive LE, it is becoming increasingly apparent that invasive cancer cells recycle several receptors, including integrins, from this compartment. We recently demonstrated that α5β1 integrin traffics to the plasma membrane from a Rab7- and WASH-positive compartment to promote invasion (Zech et al., 2011), that Rab25 and CLIC3 promote the recycling of α5β1 integrin from the late endosomal/lysosomal compartment, and that this has implications for pancreatic cancer metastasis and poor prognosis (Dozynkiewicz et al., 2012). It is thus emerging that trafficking from the LE compartment of both integrins and MT1-MMP is an important driver of invasive migration. Taking advantage of a PA-mCherry-MT1-MMP probe, we have shown that MT1-MMP traffics to the nearby plasma membrane from Rab7 containing LE/LY. Ideally, we would have liked to focus here on delivery to specific actin puncta in pseudopods, but the PA-mCherry-MT1-MMP probe was not bright enough to visualize specific delivery to pseudopod tips. Thus it remains for the future to determine how N-WASP affects polarized vesicle delivery into invasive pseudopods and whether these vesicles dock specifically at actin hotspots or whether the MT1-MMP is later captured at these sites.

N-WASP–depleted cells degraded quantitatively less collagen or native peritoneal BM than control cells in multiple assays (Fig. 5). Surprisingly though, N-WASP depletion did not affect the overall expression of MT1-MMP, its surface expression level, proteolytic processing, or the rate of internalization or recycling. Rather, depletion of N-WASP led to loss of prominent clustered actin-rich hotspots in invasive pseudopodia during 3D invasion and to increased mobility of the major collagenase MT1-MMP in the plasma membrane. Although MT1-MMP is generally localized in internal vesicles and on the plasma membrane, we could clearly see enrichment of MT1-MMP in actin hotspots (Fig. 6 B), and we observed trafficking of small mCherry-MT1-MMP vesicles into invasive pseudopods (Fig. S4). We were surprised by how relatively immobile MT1-MMP was in the plasma membrane of invading pseudopods, with only 5% exchanging within 1 min of photobleaching. But previous studies have already highlighted that receptor mobility in a 3D environment can be significantly different from what is observed in a 2D tissue culture models (Serrels et al., 2009). Depletion of N-WASP or loss of the MT1-MMP cytoplasmic tail increased the mobility of the receptor two- to threefold and caused a concomitant reduction of invasive migration and matrix remodeling capacity. We did not observe a direct interaction between N-WASP and MT1-MMP by coimmunoprecipitation (unpublished data), but rather we found that the cytoplasmic tail of MT1-MMP contained a filamentous actin-binding sequence that regulated MT1-MMP mobility in pseudopodia. Loss of this sequence ablated actin interaction and invasive matrix remodeling while increasing MT1-MMP mobility in the invasive pseudopod. Restoration using an actin-binding motif from ezrin rescued the stabilization of MT1-MMP and degradative capacity of cells.

Recently, a mechanism for recruitment of MT1-MMP to a new form of degradative focal adhesions has been proposed that is dependent on a p130Cas–FAK complex through interaction with the MT1-MMP cytoplasmic tail (Wang and McNiven, 2012). However, in this study, disruption of the MT1–MMP–p130Cas–FAK complex function solely impaired MT1-MMP–mediated degradation at focal adhesions, but not invadopodia, which suggests that a different machinery might be responsible for targeting MT1-MMP to invadopodia-like structures, at least in 2D. In contrast, other laboratories have reported p130Cas and FAK, as well as vinculin and paxillin, at invadopodia sites (Alexander et al., 2008; Branch et al., 2012), and shown that p130Cas and FAK are mechanosensitive proteins involved in invadopodia maturation and responsiveness to myosin-II activity. FAK has also been identified as a negative regulator of invadopodia in MTLn3 breast cancer cells (Chan et al., 2009), where focal adhesions and invadopodia may compete for the same tyrosine phosphorylated proteins. In our CIA, where cells contacted both Matrigel and a glass substratum, we observed that the majority of small puncta contacting matrix in invasive pseudopods also contained FAK and vinculin (Fig. S3). This suggests that in our 3D experimental conditions, hybrid structures form, which have elements of both focal adhesions and invadopodia. Clearly, various cell types have different requirements for vinculin, FAK, and p130Cas and invadopodia for invasion and invadopodia assembly. Evidence indicates that hybrid focal adhesion/invadopodia structures involving these molecules can drive invasive behavior in 3D and that sometimes seemingly contradicting results (Alexander et al., 2008; Chan et al., 2009; Wang and McNiven, 2012) about the role of focal adhesion molecules in invasion probably reflect the complexity of the system and the

Alexa Fluor 488–conjugated gelatin (green). The percentage of cells showing matrix degradation was quantified after 3 h incubation. At least 30 cells of each expressing construct were imaged for quantification from three independent experiments. Bar, 10 µm.

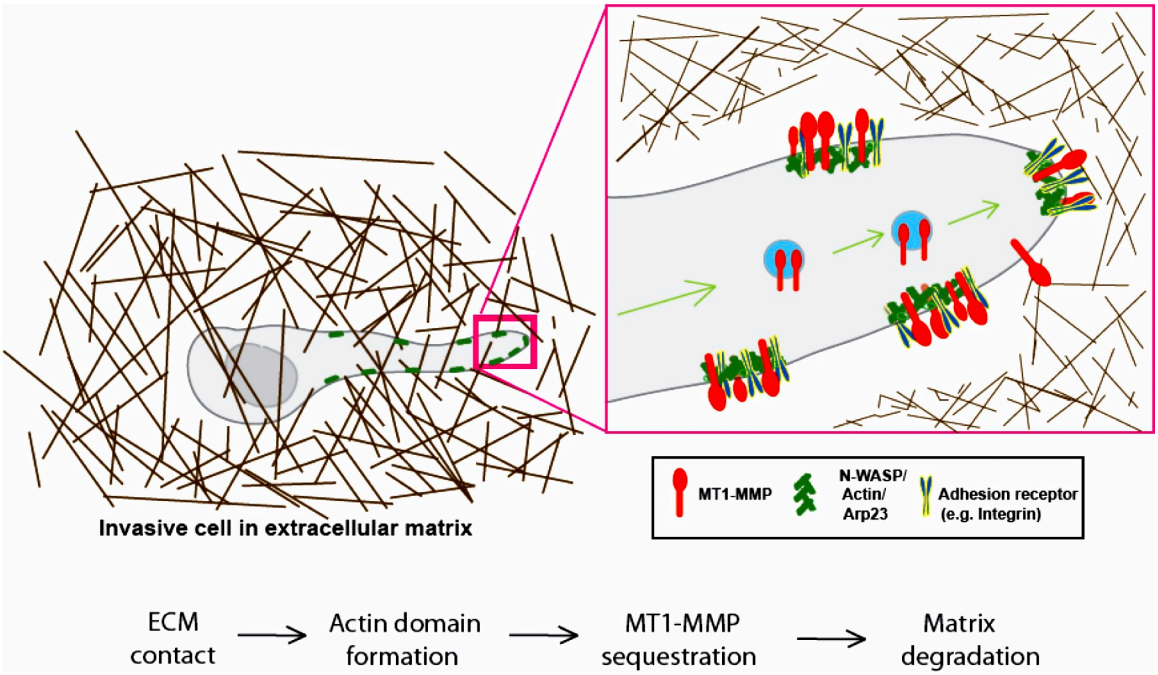

Figure 9. **Model of how N-WASP, MT1-MMP, and F-actin coordinate to function during cell invasion in 3D matrices.** N-WASP localizes to and concentrates at the front of invading pseudopods, where it polymerizes F-actin (green) to form actin-rich hotspots that also contain cortactin and Arp2/3 complex. MT1-MMP (red) was delivered via LE/lysosomal trafficking to the plasma membrane, where it is captured and anchored by F-actin. MT1-MMP becomes enriched at degradation sites by interacting with actin patches.

large number of factors that impact on whether a cell can migrate efficiently or degrade matrix.

The short cytoplasmic tail of MT1-MMP (20 aa) has previously been shown to directly interact with the µ2 subunit of the clathrin adaptor complex AP2 via a dileucine motif LL^{572}. However, interfering with internalization of MT1-MMP using aptamer peptides did not inhibit invasive migration (Wickramasinghe et al., 2010). Our data strongly suggest that N-WASP does not significantly regulate the overall levels or endocytic trafficking of MT1-MMP (Fig. S2) but rather controls the spatial organization and proper positioning of MT1-MMP with respect to active actin-based protrusions. We provide evidence that coupling to the actin cytoskeleton makes MT1-MMP more effective at degrading matrix at contact sites, and this is supported by previous observations of invadopodia-like structures forming specifically at places where invading cells encounter barriers to migration (Wolf et al., 2007; Wolf and Friedl, 2009). This is also supported by Hoshino et al. (2012), who used FRAP experiments and observed slower mobility of MT1-MMP at invadopodia than at other regions of the plasma membrane. We propose a model whereby N-WASP generates actin networks in invasive pseudopodia, where MT1-MMP is handed over from cargo vesicles (Fig. 9) to actin-rich regions of pseudopodia generated by N-WASP. Once MT1-MMP is resident in invading pseudopodia, it is then specifically stabilized by actin networks to make degradation more effective for coupling with invasion (Fig. 9).

Materials and methods

Cell culture and transfection

All reagents used for cell culture were purchased from Invitrogen unless otherwise indicated. MDA-MB-231 breast adenocarcinoma cells were obtained from the American Type Culture Collection and grown in complete DME supplemented with 10% FBS and 2 mM L-glutamine. Cells were grown in a humidified incubator with 5% CO_2 at 37°C. DNA plasmids and siRNA were transfected using the Amaxa "Nucleofector" system (Solution V, Program X-013; Lonza), according to the manufacturer's instructions.

Antibodies and reagents

We diluted antibodies 1:1,000 for Western blotting and 1:200 for immunofluorescence. Antibodies were obtained from the following sources: Altas (Sigma-Aldrich), rabbit polyclonal anti–N-WASP (HPA005750); Millipore, mouse monoclonal anti-cortactin (4F11), rabbit polyclonal anti-p34-Arc (ARPC2), and mouse monoclonal anti-MT1-MMP (MAB3328); BD, rabbit polyclonal anti-Rab7; Ambion, monoclonal mouse anti-GAPDH; Santa Cruz Biotechnology, Inc., polyclonal rabbit anti-EGFR; Invitrogen, rhodamine phalloidin, anti–mouse IgG, anti–rabbit IgG Alexa Fluor antibody, and DQ collagen; Jackson ImmunoResearch Laboratories, HRP–conjugated secondary antibodies; GenScript, >90% purity biotinylated MT1-MMP cytoplasmic tail peptides. The human issue microarray was obtained from Biomax (catalog no. Z7020004).

Immunoblotting

Cells processed for Western blotting were lysed in RIPA buffer (50 mM Tris-HCl, 150 mM NaCl, 1% NP-40, and 0.25% sodium deoxycholate) with protease inhibitor cocktail (Thermo Fisher Scientific). After SDS-PAGE and transfer to polyvinylidene fluoride membranes (GE Healthcare), ECL chemiluminescence detection kits (Thermo Fisher Scientific) were used to detect proteins of interest according to the manufacturer's instructions and with appropriate HRP-conjugated secondary antibody (1:10,000 dilution). Western blot images were recorded and processed using GeneSnap software and Bio-imaging system (Syngene). Western blots are representative of at least three repeats showing typical levels of knockdown. Quantification of Western blots was done using ImageJ to outline the bands on the blots and measure the pixel density.

Constructs and siRNAs

The plasmid containing mCherry-MT1-MMP was a gift from P. Chavrier (Institute Curie, Paris, France). GFP-Rab4 was a gift from G. Gould (University of Glasgow, Scotland, UK). GFP-Rab7 and GFP-CD151 were obtained from Addgene and GFP-LAMP1 was obtained from Origene. GFP-Lifeact and RFP-Lifeact were gifts from R. Wedlich-Soldner (AG Cellular Dynamics

and Cell Patterning, Max Planck Institute of Biochemistry, Martinsried, Germany; Riedl et al., 2008). The PA-mCherry vector was a gift from V. Verkhusha (Department of Anatomy and Structural Biology and Gruss-Lipper Biophotonics Center, Albert Einstein College of Medicine, New York, NY; Subach et al., 2009). mCherry was replaced with PA-mCherry in the previously described mCherry-MT1-MMP construct (Steffen et al., 2008). Primers to generate the MT1-MMPΔCT and ezrin actin-binding domain fusion constructs from MT1-MMP are 5′-CTTGCAGTCTTCTTCTTC-3′ and 5′-CTTGCAGTCTTCTTCATCCACAACGAGAAC-3′, respectively. N-WASP siRNA oligo #1 was from QIAGEN, the target sequence is 5′-CAGATACGACAGGGTATCCAA-3′; N-WASP siRNA oligo #2 was obtained from Thermo Fisher Scientific, the target sequence is 5′-TAGAGAGGGTGCTCAGCTAAA-3′. N-WASP shRNA was from Open Biosystems clone ID V2HS_244163. NT control siRNA and ON-TARGETplus SMARTpool siRNA targeting MT1-MMP were purchased from Thermo Fisher Scientific. Oligos targeting the noncoding sequence of MT1-MMP were obtained from QIAGEN, and the target sequences are MT1-MMP siRNA oligo #1, 5′-GACAGCGGTCTAGGAATTCAA-3′; and MT1-MMP siRNA oligo #4, 5′-CACAAGGACTTTGCCTCTGAA-3′.

Histochemistry staining and scoring of TMA

The weighted histoscore is calculated using the following formula: (0 × percentage of negative staining) + (1 × percentage of weak staining) + (2 × percentage of moderate staining) + (3 × percentage of strong staining). This gives a value between 0 and 300. This value represents the staining intensity of each core of TMA (Kirkegaard et al., 2006).

Confocal live cell imaging

MDA-MB-231 cells transfected with mCherry-MT1-MMP together with GFP-Lifeact, GFP-Rab7, GFP-CD151, GFP-LAMP1, or GFP-Rab4 were set up for CIA supplied with DME (supplemented with 10% FBS and 1% glutamine). Cells were imaged with an inverted confocal microscope (Fluoview FV1000; Olympus) equipped with a uPlan-SApochromat 60×/1.35 NA oil objective lens in an atmosphere of 5% CO_2 at 37°C. The images were collected with a photomultiplier tube (PMT) in place, using the acquisition software FV10-ASW1.7. The images were captured every 10 s for 30, 50, or 90 frames in multiple experiments. FRAP analysis of cells in CIA was performed using the same microscope with pixel resolution 512 × 512 and 2% power of 488 nm and 561 nm laser power. Effective photobleaching of mCherry was achieved using 70% of 405 nm laser power, 10 µs/pixel dwell time, and a 300-ms bleach time. Images were captured every 2 s for 30 frames.

Invasion assays

Inverted invasion assays were performed as described previously (Hennigan et al., 1994). In brief, Matrigel (BD) was diluted with PBS to 5 mg/ml and polymerized in transwell inserts (Corning) at 37°C for at least 1 h. Inserts were then inverted, and 5×10^4 cells were seeded directly onto the outside surface of the filter. For experiments with GFP- and RFP-expressing cells, RFP-labeled cells were depleted with N-WASP using siRNA oligos. 2.5×10^4 cells of each fluorescent cells were thoroughly mixed and applied to the filter. Serum-free medium was finally added to transwell inserts, and medium supplemented with 10% FBS and 25 ng/ml EGF was added atop the Matrigel. Invading cells were stained with Calcein-AM (Invitrogen) for 1 h at 72–96 h after seeding. Cells failing to cross the filter were removed with tissue, and confocal microscopy was used to visualize cells that crossed through the filter. Serial optical sections were captured at 10- or 15-µm intervals using an inverted confocal microscope (Fluoview FV1000) fitted with a uPlan-SApochromat 60×/1.35 NA oil objective lens. The confocal microscope was equipped with PMT, and the acquisition software was FV10-ASW1.7. The obtained images were analyzed and reconstructed with Volocity software. We measured the fluorescence intensity for each section using the ImageJ plugin Area Calculator. For experiments with GFP- and RFP-expressing cells, the fluorescence intensity of GFP and RFP channels were quantified and added up for each section to obtain the fluorescence intensity. Finally, the relative index of invasion was calculated as the fluorescence intensity of cells that had invaded beyond 30 µm versus the total fluorescence intensity of all cells captured in the sections imaged. At least three independent experiments were performed using duplicate samples. For immunofluorescence imaging, samples were fixed in 4% formaldehyde for 30 min, followed by washing and permeabilization with 0.1% Triton X-100 for 30 min. Samples were then washed and stained with rhodamine phalloidin and DAPI overnight at 4°C and subsequently washed three times with PBS.

Fluorescence resonance energy transfer detection by FLIM analysis

MD-MB-231 cells were prepared for CIA as mentioned but incubated in 20 mM Hepes-containing medium. Fluorescence resonance energy transfer was detected with a LIFA System (Lambert Instruments) on an inverted microscope (Eclipse TE 2000-U; Nikon) equipped with a Yokogawa CSU 22 confocal scanner unit and a modulated 60-mW 488-nm laser (Deepstar; Omicron) as a light source, which, in combination with the modulated intensifier from the LIFA system, allows measurement of fluorescence lifetimes using frequency domain. Lifetime images were acquired using the standard 488-nm filter set integrated in the spinning disk scan head. Standard halogen illumination in combination with filter blocks for GFP (470/40×, T495LP, 525/50M) or RFP (560/40×, 585LP, 632/60M) were used to check the samples for expression of the probes. Erythrosine was used as reference standard with a known lifetime of 0.086 ns. Donor (D) lifetime, τ, was analyzed using the FLIM software (version 1.2.1; Lambert Instruments).

Time-lapse microscopy with modified CIA

For the CIA method, "wounds" were created by placing a silicon self-stick cellular stopper (Thermo Fisher Scientific) in the center of a 35-mm glass bottom dish (Ibidi) before seeding 6×10^5 MDA-MB-231 cells. After 16 h, 5 mg/ml of Matrigel diluted in PBS was overlaid onto the "wounded" cell monolayer to create a matrix barrier against the cellular surface and allowed to polymerize for 2 h before adding growth medium on the top of the set Matrigel. The wounded monolayer, with overlaid Matrigel and DME (Invitrogen), supplemented with 10% FBS and 1% glutamine, was then imaged with a time-lapse microscope (TE 2000; Nikon) with a Plan-Fluor 10× objective lens (Nikon). The cells were incubated in a humidified atmosphere of 5% CO_2 at 37°C for 24 h or longer for real-time imaging with a charge-coupled device camera (CoolSnap HQ2; Photometrics) equipped with an PFS (Perfect Focus System) device before fixation and immunofluorescence. The imaged cells were tracked using ImageJ plugin Manual Tracking, and the tracking results were analyzed using the ImageJ plugin Chemotaxis Tool to calculate cell speed and persistence. Persistence was calculated as the ratio between the Euclidean distance and the total distance traveled, with a value of 1 equal to a cell traveling in a straight line. This quantification was done in least three independent experiments for each assay.

Type-I collagen film degradation assay

A collagen film assay was performed as described in a previous study, with modifications (Sabeh et al., 2004). In brief, 200 µl FITC conjugated type I collagen (Sigma-Aldrich) was distributed evenly on glass-bottom microwell dishes (14-mm microwell; MatTek) and allowed to dry for 2–3 h to form a uniform collagen film. 5×10^4 MDA-MB-231 cells were seeded to the collagen film and incubated for 48 h. Cells then were fixed and labeled with rhodamine phalloidin and DAPI (Molecular Probes). Images were captured with a confocal microscope (Fluoview FV1000) fitted with a uPlan-SApochromat 60×/1.35 NA oil objective lens. The confocal microscope was equipped with a PMT to capture images, and the acquisition software was FV10-ASW1.7.

Quantitative 3D collagen degradation assay

A 3D collagen degradation assay was performed as described previously, with modifications (Wolf and Friedl, 2009). In brief, CHL-1 cells treated with NT, N-WASP, MT1-MMP siRNA, or 5 µM GM6001 MMP inhibitor were embedded into collagen I lattices (BD) containing DQ-FITC–labeled type I collagen monomers (2%; Molecular Probes). After 40 h of culture, solid-phase collagen including cells was pelleted, and the supernatant containing released FITC-collagen fragments was analyzed spectrofluorimetrically (QuantaMasterTM 40 spectrofluorometer; Photon Technology International). The degradation of fibrillar collagen for each sample was calculated as fluorescence released from DQ-FITC–labeled type I collagen monomers subtracted by background fluorescence, which was calculated by pelleting nondigested cell-free collagen lattices. Quantification of degradation was done in at least three independent experiments in duplicate for each assay.

Quantification of cell length/width ratio

To measure cell length/width ratio (Fig. 3 B), at least 30 confocal images of cells stained with rhodamine phalloidin and DAPI were captured. To obtain the length of cells, we drew a line from rear point of the main cell body passing the center of nucleus to the tip of the longest pseudopod, which was defined as the cell length. For the cell width, we drew a line passing the center of the nucleus that crosses the widest point of cell main body. The ratio of length/width reflects cell morphology in CIA. This quantification was done in at least three independent experiments for each assay.

Invadopodia gelatin degradation assay

Invadopodia gelatin degradation assays were performed as described previously (Artym et al., 2006). In brief, coverslips were acid-washed and coated with 50 µg/ml poly-L-lysine for 15 min, washed with PBS, and cross-linked with 0.5% glutaraldehyde for 15 min. The coverslips were then inverted

on an 80-µl drop of 1 mg/ml Alexa Fluor 488–conjugated gelatin (Invitrogen) for 10 min. After washing with PBS, the coverslips were then quenched with 5 mg/ml sodium borohydride for 3 min followed by another washing with PBS. Finally coverslips were sterilized with 70% ethanol for 5 min and incubated in complete growth medium for 1 h before use. To assess the ability of cells to form invadopodia, cells were cultured on cross-linked fluorescent conjugated matrix for 3 h. The percentage of cells showing degradation was quantified and shown in a bar graph.

BM degradation and transmigration assay

Peritoneal BM was prepared as previously described (Witz et al., 2001; Hotary et al., 2006). In brief, the peritoneal BM was isolated by stripping the overlying mesothelial cells from C57BL/6 mouse mesentery using 1 N ammonium hydroxide and mounting the isolated mesentery on 6.5-mm diameter Transwells (BD). After washing with PBS, 5×10^4 MDA-MB-231 cells were seeded on the top of the BMs in DME supplemented with 10% FBS. 1 ml of medium was placed in the lower chambers. After 3 d of culture, the samples were fixed in 4% formaldehyde and stained for collagen IV on both sides. BM and cells were visualized with an inverted confocal microscope fitted with a uPlan-SApochromat 60×/1.35 NA oil objective lens (Fluoview FV1000; Olympus). The confocal microscope was equipped with a PMT to capture images, and the acquisition software was FV10-ASW1.7. To quantify remaining collagen IV staining, z-stack images of 10 BM areas were collected from the top of the BM to the bottom. The extended focus projection images of z stacks were used to analyze the total staining of collagen IV. Quantification was done in at least three independent experiments in duplicate for each assay.

Cell surface biotinylation and MT1-MMP trafficking assays

Cell surface proteins were biotinylated by incubating the cells with 0.5 mg/ml sulfo-NHS-SS-biotin (Pierce) as described previously (Le et al., 1999). Cleared cell lysate containing 400 µg of total protein from each sample was incubated with NeutrAvidin Agarose Resin (Thermo Fischer Scientific) to pull down biotinylated proteins. The samples were then analyzed by immunoblotting for MT1-MMP or EGFR. Three independent experiments have been performed on three occasions.

MT1-MMP internalization and recycling assays were performed as described previously for integrins (Roberts et al., 2001), with the following modifications: monoclonal mouse anti–MT1-MMP (MAB3328) was used to coat the ELISA plates at 5 µg/ml at 4C° overnight. MDA-MB-231 cells were not serum-starved; receptor internalization conditions for recycling were 30 min at 37°C; 10 µg/ml collagen was added to the cells during the internalization and recycling periods. In brief, cells were cooled on ice with ice-cold PBS and labeled with 0.2 mg/ml NHS-SS-biotin (Pierce) for 30 min on a rocker at 4°C. Labeled cells were washed two times with cold PBS on ice and transferred to 37°C medium in the presence (for internalization experiments only) or absence of 0.6 µM primaquine for the indicated times. Medium was aspirated and the cells were rapidly cooled down on ice with the addition of ice-cold PBS. Remaining cell surface biotin was removed with 20 mM MesNa in 50 mM Tris, pH 8.6, and 100 mM NaCl for 15 min on a rocker at 4°C. The reaction was quenched with 20 mM iodoacetamide for 10 min, and, subsequently, cells were lysed and centrifuged, and 50 µl of postnuclear supernatant was plated on the prepared antibody-coated 96-well plated and incubated overnight at 4°C.

F-actin sedimentation assay

Rabbit muscle actin was purified as described previously (Spudich and Watt, 1971; Machesky and Hall, 1997). In brief, muscle acetone powder was extracted in 20 ml G buffer (2 mM Tris, pH 8, 0.2 mM ATP, 0.5 mM DTT, and 0.2 mM $CaCl_2$) per gram of acetone powder on ice for 30 min. This was sedimented for 30 min at 30,000 *g* at 2°C, and the extraction step followed by centrifugation was repeated. The combined supernatants were made up to 50 mM KCl and 2 mM $MgCl_2$, and the solution was stirred at room temperature for 30 min and then on ice for 30 min. Finally, the solution was brought up to 0.8 M KCl and stirred for a further 30 min on ice before sedimentation at 100,000 *g* for 2 h at 4°C. The pellets were resuspended in G buffer with Dounce homogenization and dialyzed for 2 d into G buffer, then sedimented for 2 h at 100,000 *g* to pellet the oligomers. The top two thirds of the supernatant was removed and used as G-actin. MT1-MMP cytoplasmic tail peptides were solubilized in G buffer at 2 µg/µl. Cytoplasmic tail peptides (final concentration, 25 µm) in G buffer were mixed with the indicated concentrations of G-actin, brought to a final concentration of 0.1 KCl to allow F-actin polymerization, and incubated for 1 h at room temperature. Suspensions were pelleted for 1 h at 100,000 *g* 4°C in a Beckman table-top ultracentrifuge. Pellets and supernatants were brought to a volume of 100 µl with NuPAGE samples buffer, and 10 µl were run on a 4–12% NuPAGE gel.

Steady-state fluorescence anisotropy experiments

The steady-state fluorescence anisotropy measurements were performed with a Jobin Yvon (HORIBA) spectrofluorometer equipped with a thermostable cuvette holder. The experiments were performed at pH 8.0 in a buffer containing 2 mM Tris/HCl, 0.2 mM ATP, 0.005% NaN_3, 0.5 mM 2-mercaptoethanol, 100 mM KCl, and 2 mM $CaCl_2$ (buffer F). The excitation wavelength for 5-({2-[(iodoacetyl)amino]ethyl}amino)naphthalene-1-sulfonic acid (IAEDANS) was 350 nm, and the fluorescence anisotropy of the IAEDANS was recorded at 490 nm. The optical slits were set to 5 nm in both the excitation and emission side. Actin was labeled with IAEDANS fluorescent probes on Cys374 (Visegrády et al., 2004). The labeling ratio (the probe concentration vs. actin concentration) for IAEDANS was 0.9.

We have used a quadratic equation to fit the binding data and calculate the K_d: $[PL]/[P] = (([P] + [L] + K_d) - (([P] + [L] + K_d)^2 - 4 \times [P] \times [L])^{0.5})/2 \times [L]$, where [PL] is the concentration of the peptide bound to actin, [L] is the total concentration of the peptide, which is varied, [P] is the total concentration of actin, and [PL]/[P] is the fraction of ligand bound to receptor.

Online supplemental material

Fig. S1 shows that depletion of N-WASP does not affect cell migration on a 2D rigid surface, and also shows representative knockdowns of N-WASP and normal migration parameters when cells are on a rigid 2D surface. Fig. S2 shows that depletion of N-WASP has no effects on MT1-MMP levels, endocytosis, or recycling rates. Also shown are Western blots of MT1-MMP levels and the results of endocytosis and recycling assays using biotinylated surface labeling of MT1-MMP. Fig. S3 shows that the focal adhesion proteins vinculin and FAK partially colocalize with invadopodia-like structures in CIA. The figure also shows cells migrating in the CIA and morphology of focal adhesions and invadopodia-like structures. Fig. S4 shows that MT1-MMP colocalizes to LE/LY but not EE compartments. The figure also shows still images from movies of MT1-MMP colocalizing with late endocytic but not early endocytic compartments, and shows preferential localization of MT1-MMP–containing vesicles to the leading half of cells migrating in CIA. Fig. S5 shows MT1-MMP cytoplasmic tail mutant expression and the effect on cell invasion in CIA and mobility in FRAP. The figure also shows a Western blot of expression levels of MT1-MMP and mutants in cells depleted of endogenous MT1-MMP but rescued with mutants. Also shown is the lack of rescue of invasion in CIA when MT1-MMP knockdown is replaced with LLY/AAA mutant and various control FRAP experiments of MT1-MMP in pseudopodia of cells invading in CIA. Video 1 shows 3D reconstruction of MDA-MB-231 cells invading into Matrigel in 3D invasion assay, corresponding to Fig. 2 B. Video 2 shows a 3D reconstruction of N-WASP knockdown MDA-MB-231 cells invading into Matrigel in a 3D invasion assay corresponding to Fig. 2 B. Video 3 shows migration of cells invading in CIA with control and N-WASP knockdown, corresponding to stills in Fig. 3 A. Video 4 shows invasive migration of cells in CIA in various concentrations of Matrigel, corresponding to Fig. 3 B. Video 5 shows colocalization of mCherry-MT1-MMP with GFP-Rab7 corresponding to stills shown in Fig. S4 A. Video 6 shows photoactivated MT1-MMP trafficking from a Rab7-positive LE to the plasma-membrane, corresponding to still images in Fig. 6 D. Video 7 shows mCherry-MT1-MMP vesicles trafficking into invading pseudopods in NT cells while invading in CIA, but not in N-WASP knockdown cells, and corresponds to stills shown in Fig. S4 B. Online supplemental material is available at http://www.jcb.org/cgi/content/full/jcb.201203025/DC1.

We thank Drs. Stephen Weiss (University of Michigan) and Gareth Jones (King's College London) for helpful advice and for comments on our manuscript. We thank Prof. Barry Gusterson (Glasgow University) for helpful advice and for help with the breast cancer TMA scoring.

We thank Kurt Anderson, Margaret O'Prey, and Tom Gilbey of the Beatson Advanced Imaging Resource imaging facility for help with imaging. L.M. Machesky, J.C. Norman, and R.H. Insall thank Cancer Research UK for core funding. L.M. Machesky and X. Yu were also funded by the Medical Research Council UK on a Research Senior Fellowship G117/569 to L.M. Machesky, and X. Yu is currently funded by Association for International Cancer Research grant 11-0119 to L.M. Machesky.

Submitted: 7 March 2012
Accepted: 28 September 2012

References

Alexander, N.R., K.M. Branch, A. Parekh, E.S. Clark, I.C. Iwueke, S.A. Guelcher, and A.M. Weaver. 2008. Extracellular matrix rigidity promotes invadopodia activity. *Curr. Biol.* 18:1295–1299. http://dx.doi.org/10.1016/j.cub.2008.07.090

Artym, V.V., Y. Zhang, F. Seillier-Moiseiwitsch, K.M. Yamada, and S.C. Mueller. 2006. Dynamic interactions of cortactin and membrane type 1 matrix metalloproteinase at invadopodia: defining the stages of invadopodia formation and function. *Cancer Res.* 66:3034–3043. http://dx.doi.org/10.1158/0008-5472.CAN-05-2177

Benesch, S., S. Lommel, A. Steffen, T.E. Stradal, N. Scaplehorn, M. Way, J. Wehland, and K. Rottner. 2002. Phosphatidylinositol 4,5-biphosphate (PIP2)-induced vesicle movement depends on N-WASP and involves Nck, WIP, and Grb2. *J. Biol. Chem.* 277:37771–37776. http://dx.doi.org/10.1074/jbc.M204145200

Branch, K.M., D. Hoshino, and A.M. Weaver. 2012. Adhesion rings surround invadopodia and promote maturation. *Biology Open*. 1:711–722. http://dx.doi.org/10.1242/bio.20121867

Bravo-Cordero, J.J., R. Marrero-Diaz, D. Megías, L. Genís, A. García-Grande, M.A. García, A.G. Arroyo, and M.C. Montoya. 2007. MT1-MMP proinvasive activity is regulated by a novel Rab8-dependent exocytic pathway. *EMBO J.* 26:1499–1510. http://dx.doi.org/10.1038/sj.emboj.7601606

Bryce, N.S., E.S. Clark, J.L. Leysath, J.D. Currie, D.J. Webb, and A.M. Weaver. 2005. Cortactin promotes cell motility by enhancing lamellipodial persistence. *Curr. Biol.* 15:1276–1285. http://dx.doi.org/10.1016/j.cub.2005.06.043

Bu, W., A.M. Chou, K.B. Lim, T. Sudhaharan, and S. Ahmed. 2009. The Toca-1-N-WASP complex links filopodial formation to endocytosis. *J. Biol. Chem.* 284:11622–11636. http://dx.doi.org/10.1074/jbc.M805940200

Caldieri, G., I. Ayala, F. Attanasio, and R. Buccione. 2009. Cell and molecular biology of invadopodia. *Int Rev Cell Mol Biol*. 275:1–34. http://dx.doi.org/10.1016/S1937-6448(09)75001-4

Chan, K.T., C.L. Cortesio, and A. Huttenlocher. 2009. FAK alters invadopodia and focal adhesion composition and dynamics to regulate breast cancer invasion. *J. Cell Biol.* 185:357–370. http://dx.doi.org/10.1083/jcb.200809110

Chun, T.H., K.B. Hotary, F. Sabeh, A.R. Saltiel, E.D. Allen, and S.J. Weiss. 2006. A pericellular collagenase directs the 3-dimensional development of white adipose tissue. *Cell*. 125:577–591. http://dx.doi.org/10.1016/j.cell.2006.02.050

Clark, E.S., A.S. Whigham, W.G. Yarbrough, and A.M. Weaver. 2007. Cortactin is an essential regulator of matrix metalloproteinase secretion and extracellular matrix degradation in invadopodia. *Cancer Res.* 67:4227–4235. http://dx.doi.org/10.1158/0008-5472.CAN-06-3928

Desmarais, V., H. Yamaguchi, M. Oser, L. Soon, G. Mouneimne, C. Sarmiento, R. Eddy, and J. Condeelis. 2009. N-WASP and cortactin are involved in invadopodium-dependent chemotaxis to EGF in breast tumor cells. *Cell Motil. Cytoskeleton*. 66:303–316. http://dx.doi.org/10.1002/cm.20361

Dozynkiewicz, M.A., N.B. Jamieson, I. Macpherson, J. Grindlay, P.V. van den Berghe, A. von Thun, J.P. Morton, C. Gourley, P. Timpson, C. Nixon, et al. 2012. Rab25 and CLIC3 collaborate to promote integrin recycling from late endosomes/lysosomes and drive cancer progression. *Dev. Cell*. 22:131–145. http://dx.doi.org/10.1016/j.devcel.2011.11.008

Fisher, K.E., A. Sacharidou, A.N. Stratman, A.M. Mayo, S.B. Fisher, R.D. Mahan, M.J. Davis, and G.E. Davis. 2009. MT1-MMP- and Cdc42-dependent signaling co-regulate cell invasion and tunnel formation in 3D collagen matrices. *J. Cell Sci.* 122:4558–4569. http://dx.doi.org/10.1242/jcs.050724

Fluck, M.M., and B.S. Schaffhausen. 2009. Lessons in signaling and tumorigenesis from polyomavirus middle T antigen. *Microbiol. Mol. Biol. Rev.* 73:542–563. http://dx.doi.org/10.1128/MMBR.00009-09

Frittoli, E., A. Palamidessi, A. Disanza, and G. Scita. 2011. Secretory and endo/exocytic trafficking in invadopodia formation: the MT1-MMP paradigm. *Eur. J. Cell Biol.* 90:108–114. http://dx.doi.org/10.1016/j.ejcb.2010.04.007

Gligorijevic, B., J. Wyckoff, H. Yamaguchi, Y. Wang, E.T. Roussos, and J. Condeelis. 2012. N-WASP-mediated invadopodium formation is involved in intravasation and lung metastasis of mammary tumors. *J. Cell Sci.* 125:724–734. http://dx.doi.org/10.1242/jcs.092726

Hennigan, R.F., K.L. Hawker, and B.W. Ozanne. 1994. Fos-transformation activates genes associated with invasion. *Oncogene*. 9:3591–3600.

Hoshino, D., N. Koshikawa, T. Suzuki, V. Quaranta, A.M. Weaver, M. Seiki, and K. Ichikawa. 2012. Establishment and validation of computational model for MT1-MMP dependent ECM degradation and intervention strategies. *PLOS Comput. Biol.* 8:e1002479. http://dx.doi.org/10.1371/journal.pcbi.1002479

Hotary, K., X.Y. Li, E. Allen, S.L. Stevens, and S.J. Weiss. 2006. A cancer cell metalloprotease triad regulates the basement membrane transmigration program. *Genes Dev.* 20:2673–2686. http://dx.doi.org/10.1101/gad.1451806

Hüfner, K., B. Schell, M. Aepfelbacher, and S. Linder. 2002. The acidic regions of WASp and N-WASP can synergize with CDC42Hs and Rac1 to induce filopodia and lamellipodia. *FEBS Lett.* 514:168–174. http://dx.doi.org/10.1016/S0014-5793(02)02358-X

Isaac, B.M., D. Ishihara, L.M. Nusblat, J.C. Gevrey, A. Dovas, J. Condeelis, and D. Cox. 2010. N-WASP has the ability to compensate for the loss of WASP in macrophage podosome formation and chemotaxis. *Exp. Cell Res.* 316:3406–3416. http://dx.doi.org/10.1016/j.yexcr.2010.06.011

Jiang, A., K. Lehti, X. Wang, S.J. Weiss, J. Keski-Oja, and D. Pei. 2001. Regulation of membrane-type matrix metalloproteinase 1 activity by dynamin-mediated endocytosis. *Proc. Natl. Acad. Sci. USA*. 98:13693–13698. http://dx.doi.org/10.1073/pnas.241293698

Jin, F., B. Dong, J. Georgiou, Q. Jiang, J. Zhang, A. Bharioke, F. Qiu, S. Lommel, M.L. Feltri, L. Wrabetz, et al. 2011. N-WASp is required for Schwann cell cytoskeletal dynamics, normal myelin gene expression and peripheral nerve myelination. *Development*. 138:1329–1337. http://dx.doi.org/10.1242/dev.058677

Kam, Y., C. Guess, L. Estrada, B. Weidow, and V. Quaranta. 2008. A novel circular invasion assay mimics in vivo invasive behavior of cancer cell lines and distinguishes single-cell motility in vitro. *BMC Cancer*. 8:198. http://dx.doi.org/10.1186/1471-2407-8-198

Kirkegaard, T., J. Edwards, S. Tovey, L.M. McGlynn, S.N. Krishna, R. Mukherjee, L. Tam, A.F. Munro, B. Dunne, and J.M. Bartlett. 2006. Observer variation in immunohistochemical analysis of protein expression, time for a change? *Histopathology*. 48:787–794. http://dx.doi.org/10.1111/j.1365-2559.2006.02412.x

Kowalski, J.R., C. Egile, S. Gil, S.B. Snapper, R. Li, and S.M. Thomas. 2005. Cortactin regulates cell migration through activation of N-WASP. *J. Cell Sci.* 118:79–87. http://dx.doi.org/10.1242/jcs.01586

Le, T.L., A.S. Yap, and J.L. Stow. 1999. Recycling of E-cadherin: a potential mechanism for regulating cadherin dynamics. *J. Cell Biol.* 146:219–232.

Legg, J.A., G. Bompard, J. Dawson, H.L. Morris, N. Andrew, L. Cooper, S.A. Johnston, G. Tramountanis, and L.M. Machesky. 2007. N-WASP involvement in dorsal ruffle formation in mouse embryonic fibroblasts. *Mol. Biol. Cell*. 18:678–687. http://dx.doi.org/10.1091/mbc.E06-06-0569

Linder, S. 2007. The matrix corroded: podosomes and invadopodia in extracellular matrix degradation. *Trends Cell Biol.* 17:107–117. http://dx.doi.org/10.1016/j.tcb.2007.01.002

Lommel, S., S. Benesch, K. Rottner, T. Franz, J. Wehland, and R. Kühn. 2001. Actin pedestal formation by enteropathogenic *Escherichia coli* and intracellular motility of *Shigella flexneri* are abolished in N-WASP-defective cells. *EMBO Rep.* 2:850–857. http://dx.doi.org/10.1093/embo-reports/kve197

Lorenz, M., H. Yamaguchi, Y. Wang, R.H. Singer, and J. Condeelis. 2004. Imaging sites of N-wasp activity in lamellipodia and invadopodia of carcinoma cells. *Curr. Biol.* 14:697–703. http://dx.doi.org/10.1016/j.cub.2004.04.008

Ludwig, T., S.M. Theissen, M.J. Morton, and M.J. Caplan. 2008. The cytoplasmic tail dileucine motif LL572 determines the glycosylation pattern of membrane-type 1 matrix metalloproteinase. *J. Biol. Chem.* 283:35410–35418. http://dx.doi.org/10.1074/jbc.M801816200

Machesky, L.M., and A. Hall. 1997. Role of actin polymerization and adhesion to extracellular matrix in Rac- and Rho-induced cytoskeletal reorganization. *J. Cell Biol.* 138:913–926. http://dx.doi.org/10.1083/jcb.138.4.913

Merrifield, C.J., M.E. Feldman, L. Wan, and W. Almers. 2002. Imaging actin and dynamin recruitment during invagination of single clathrin-coated pits. *Nat. Cell Biol.* 4:691–698. http://dx.doi.org/10.1038/ncb837

Miki, H., T. Sasaki, Y. Takai, and T. Takenawa. 1998. Induction of filopodium formation by a WASP-related actin-depolymerizing protein N-WASP. *Nature*. 391:93–96. http://dx.doi.org/10.1038/34208

Misra, A., R.P. Lim, Z. Wu, and T. Thanabalu. 2007. N-WASP plays a critical role in fibroblast adhesion and spreading. *Biochem. Biophys. Res. Commun.* 364:908–912. http://dx.doi.org/10.1016/j.bbrc.2007.10.086

Muller, W.J., E. Sinn, P.K. Pattengale, R. Wallace, and P. Leder. 1988. Single-step induction of mammary adenocarcinoma in transgenic mice bearing the activated c-neu oncogene. *Cell*. 54:105–115. http://dx.doi.org/10.1016/0092-8674(88)90184-5

Nakahara, H., L. Howard, E.W. Thompson, H. Sato, M. Seiki, Y. Yeh, and W.T. Chen. 1997. Transmembrane/cytoplasmic domain-mediated membrane type 1-matrix metalloprotease docking to invadopodia is required for cell invasion. *Proc. Natl. Acad. Sci. USA*. 94:7959–7964. http://dx.doi.org/10.1073/pnas.94.15.7959

Oser, M., H. Yamaguchi, C.C. Mader, J.J. Bravo-Cordero, M. Arias, X. Chen, V. Desmarais, J. van Rheenen, A.J. Koleske, and J. Condeelis. 2009. Cortactin regulates cofilin and N-WASp activities to control the stages of invadopodium assembly and maturation. *J. Cell Biol.* 186:571–587. http://dx.doi.org/10.1083/jcb.200812176

Peränen, J., P. Auvinen, H. Virta, R. Wepf, and K. Simons. 1996. Rab8 promotes polarized membrane transport through reorganization of actin and microtubules in fibroblasts. *J. Cell Biol.* 135:153–167. http://dx.doi.org/10.1083/jcb.135.1.153

Poincloux, R., F. Lizárraga, and P. Chavrier. 2009. Matrix invasion by tumour cells: a focus on MT1-MMP trafficking to invadopodia. *J. Cell Sci.* 122:3015–3024. http://dx.doi.org/10.1242/jcs.034561

Puthenveedu, M.A., B. Lauffer, P. Temkin, R. Vistein, P. Carlton, K. Thorn, J. Taunton, O.D. Weiner, R.G. Parton, and M. von Zastrow. 2010. Sequence-dependent sorting of recycling proteins by actin-stabilized endosomal microdomains. *Cell*. 143:761–773. http://dx.doi.org/10.1016/j.cell.2010.10.003

Riedl, J., A.H. Crevenna, K. Kessenbrock, J.H. Yu, D. Neukirchen, M. Bista, F. Bradke, D. Jenne, T.A. Holak, Z. Werb, et al. 2008. Lifeact: a versatile marker to visualize F-actin. *Nat. Methods*. 5:605–607. http://dx.doi.org/10.1038/nmeth.1220

Roberts, M., S. Barry, A. Woods, P. van der Sluijs, and J. Norman. 2001. PDGF-regulated rab4-dependent recycling of alphavbeta3 integrin from early endosomes is necessary for cell adhesion and spreading. *Curr. Biol.* 11:1392–1402. http://dx.doi.org/10.1016/S0960-9822(01)00442-0

Sabeh, F., I. Ota, K. Holmbeck, H. Birkedal-Hansen, P. Soloway, M. Balbin, C. Lopez-Otin, S. Shapiro, M. Inada, S. Krane, et al. 2004. Tumor cell traffic through the extracellular matrix is controlled by the membrane-anchored collagenase MT1-MMP. *J. Cell Biol.* 167:769–781. http://dx.doi.org/10.1083/jcb.200408028

Sarmiento, C., W. Wang, A. Dovas, H. Yamaguchi, M. Sidani, M. El-Sibai, V. Desmarais, H.A. Holman, S. Kitchen, J.M. Backer, et al. 2008. WASP family members and formin proteins coordinate regulation of cell protrusions in carcinoma cells. *J. Cell Biol.* 180:1245–1260. http://dx.doi.org/10.1083/jcb.200708123

Scott, R.W., S. Hooper, D. Crighton, A. Li, I. König, J. Munro, E. Trivier, G. Wickman, P. Morin, D.R. Croft, et al. 2010. LIM kinases are required for invasive path generation by tumor and tumor-associated stromal cells. *J. Cell Biol.* 191:169–185. http://dx.doi.org/10.1083/jcb.201002041

Seiki, M., N. Koshikawa, and I. Yana. 2003. Role of pericellular proteolysis by membrane-type 1 matrix metalloproteinase in cancer invasion and angiogenesis. *Cancer Metastasis Rev.* 22:129–143. http://dx.doi.org/10.1023/A:1023087113214

Serrels, A., P. Timpson, M. Canel, J.P. Schwarz, N.O. Carragher, M.C. Frame, V.G. Brunton, and K.I. Anderson. 2009. Real-time study of E-cadherin and membrane dynamics in living animals: implications for disease modeling and drug development. *Cancer Res.* 69:2714–2719. http://dx.doi.org/10.1158/0008-5472.CAN-08-4308

Snapper, S.B., F. Takeshima, I. Antón, C.H. Liu, S.M. Thomas, D. Nguyen, D. Dudley, H. Fraser, D. Purich, M. Lopez-Ilasaca, et al. 2001. N-WASP deficiency reveals distinct pathways for cell surface projections and microbial actin-based motility. *Nat. Cell Biol.* 3:897–904. http://dx.doi.org/10.1038/ncb1001-897

Spudich, J.A., and S. Watt. 1971. The regulation of rabbit skeletal muscle contraction. I. Biochemical studies of the interaction of the tropomyosin-troponin complex with actin and the proteolytic fragments of myosin. *J. Biol. Chem.* 246:4866–4871.

Steffen, A., G. Le Dez, R. Poincloux, C. Recchi, P. Nassoy, K. Rottner, T. Galli, and P. Chavrier. 2008. MT1-MMP-dependent invasion is regulated by TI-VAMP/VAMP7. *Curr. Biol.* 18:926–931. http://dx.doi.org/10.1016/j.cub.2008.05.044

Subach, F.V., G.H. Patterson, S. Manley, J.M. Gillette, J. Lippincott-Schwartz, and V.V. Verkhusha. 2009. Photoactivatable mCherry for high-resolution two-color fluorescence microscopy. *Nat. Methods*. 6:153–159. http://dx.doi.org/10.1038/nmeth.1298

Taunton, J., B.A. Rowning, M.L. Coughlin, M. Wu, R.T. Moon, T.J. Mitchison, and C.A. Larabell. 2000. Actin-dependent propulsion of endosomes and lysosomes by recruitment of N-WASP. *J. Cell Biol.* 148:519–530. http://dx.doi.org/10.1083/jcb.148.3.519

Uekita, T., Y. Itoh, I. Yana, H. Ohno, and M. Seiki. 2001. Cytoplasmic tail-dependent internalization of membrane-type 1 matrix metalloproteinase is important for its invasion-promoting activity. *J. Cell Biol.* 155:1345–1356. http://dx.doi.org/10.1083/jcb.200108112

Visegrády, B., D. Lorinczy, G. Hild, B. Somogyi, and M. Nyitrai. 2004. The effect of phalloidin and jasplakinolide on the flexibility and thermal stability of actin filaments. *FEBS Lett.* 565:163–166. http://dx.doi.org/10.1016/j.febslet.2004.03.096

Wang, Y., and M.A. McNiven. 2012. Invasive matrix degradation at focal adhesions occurs via protease recruitment by a FAK-p130Cas complex. *J. Cell Biol.* 196:375–385. http://dx.doi.org/10.1083/jcb.201105153

Wickramasinghe, R.D., P. Ko Ferrigno, and C. Roghi. 2010. Peptide aptamers as new tools to modulate clathrin-mediated internalisation—inhibition of MT1-MMP internalisation. *BMC Cell Biol.* 11:58. http://dx.doi.org/10.1186/1471-2121-11-58

Witz, C.A., I.A. Montoya-Rodriguez, S. Cho, V.E. Centonze, L.F. Bonewald, and R.S. Schenken. 2001. Composition of the extracellular matrix of the peritoneum. *J. Soc. Gynecol. Investig.* 8:299–304. http://dx.doi.org/10.1016/S1071-5576(01)00122-8

Wolf, K., and P. Friedl. 2009. Mapping proteolytic cancer cell-extracellular matrix interfaces. *Clin. Exp. Metastasis*. 26:289–298. http://dx.doi.org/10.1007/s10585-008-9190-2

Wolf, K., Y.I. Wu, Y. Liu, J. Geiger, E. Tam, C. Overall, M.S. Stack, and P. Friedl. 2007. Multi-step pericellular proteolysis controls the transition from individual to collective cancer cell invasion. *Nat. Cell Biol.* 9:893–904. http://dx.doi.org/10.1038/ncb1616

Yamaguchi, H., M. Lorenz, S. Kempiak, C. Sarmiento, S. Coniglio, M. Symons, J. Segall, R. Eddy, H. Miki, T. Takenawa, and J. Condeelis. 2005. Molecular mechanisms of invadopodium formation: the role of the N-WASP-Arp2/3 complex pathway and cofilin. *J. Cell Biol.* 168:441–452. http://dx.doi.org/10.1083/jcb.200407076

Yanagawa, R., Y. Furukawa, T. Tsunoda, O. Kitahara, M. Kameyama, K. Murata, O. Ishikawa, and Y. Nakamura. 2001. Genome-wide screening of genes showing altered expression in liver metastases of human colorectal cancers by cDNA microarray. *Neoplasia*. 3:395–401. http://dx.doi.org/10.1038/sj.neo.7900185

Yarar, D., C.M. Waterman-Storer, and S.L. Schmid. 2007. SNX9 couples actin assembly to phosphoinositide signals and is required for membrane remodeling during endocytosis. *Dev. Cell*. 13:43–56. http://dx.doi.org/10.1016/j.devcel.2007.04.014

Yu, X., and L.M. Machesky. 2012. Cells assemble invadopodia-like structures and invade into matrigel in a matrix metalloprotease dependent manner in the circular invasion assay. *PLoS ONE*. 7:e30605. http://dx.doi.org/10.1371/journal.pone.0030605

Zech, T., S.D. Calaminus, P. Caswell, H.J. Spence, M. Carnell, R.H. Insall, J. Norman, and L.M. Machesky. 2011. The Arp2/3 activator WASH regulates α5β1-integrin-mediated invasive migration. *J. Cell Sci.* 124:3753–3759. http://dx.doi.org/10.1242/jcs.080986